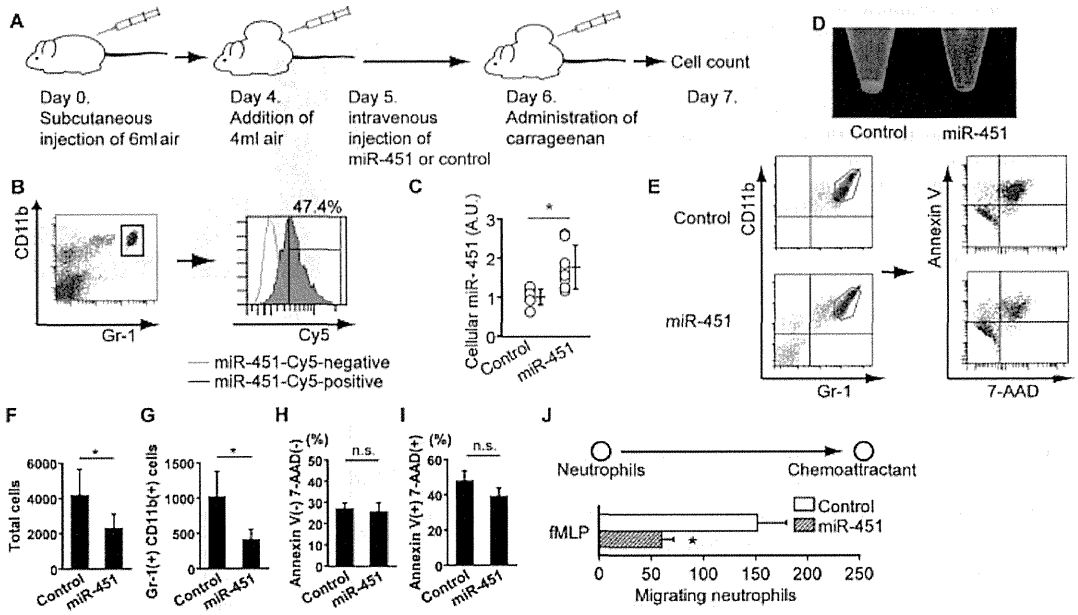

Figure 2. Overexpression of microRNA-451 (miR-451) decreases chemotaxis ability. **A,** The air-pouch model of local inflammation in BALB/c mice is shown (see Materials and Methods for details). Double-stranded miR-451 or small interfering RNA (siRNA) (as a control) was injected into the tail vein 24 hours before the carrageenan injection. **B,** Cy5+ or Cy5− miR-451 with atelocollagen was administered intravenously, and the uptake of miRNA by neutrophils in the peripheral blood was assessed by flow cytometry 24 hours later. The percentage of Cy5+ cells is indicated. **C,** Neutrophils were obtained from spleens of mice that had been treated with double-stranded miR-451 or control siRNA 24 hours before isolation. Expression of miR-451 (normalized to the expression of snoRNA202) in neutrophils was measured by real-time quantitative polymerase chain reaction. Each circle represents an individual mouse (n = 8 per group). Bars show the mean ± SD. **D,** The pellet obtained from the air-pouch lavage fluid is shown. **E–I,** Cells that had infiltrated into the lavage fluid were stained for Gr-1, CD11b, annexin V, and 7-aminoactinomycin D (7-AAD), and counted by flow cytometry. Representative flow cytometric results (**E**) and mean ± SEM cell counts (**F–I**) are shown. **J,** An under-agarose assay was used to evaluate migration of neutrophils to gradients of the chemoattractant. Neutrophils were obtained from spleens of mice that had been treated with double-stranded miR-451 or control siRNA 24 hours before isolation. Ten microliters of 0.1 μM fMLP was loaded into the outer wells of the gel. Values are the mean ± SEM of 5 independent experiments. * = $P < 0.05$. NS = not significant.

Administration of miR-451 significantly decreased infiltration by cells overall (Figures 2D–F) and by Gr-1+CD11b+ neutrophils (Figure 2G). It has been reported that miR-451 induces apoptosis via Rab14 in human non–small cell lung cancer (17). However, apoptosis did not increase in the accumulated neutrophils of miR-451–treated mice (Figures 2H and I), indicating that apoptosis was not involved in the decreased infiltration by neutrophils. There were no significant differences in the number of neutrophils in peripheral blood or in the mean fluorescence intensity of Gr-1 in the accumulated neutrophils (data not shown).

To exclude the influence of the capsule cells of the air pouch, neutrophils obtained from miR-451–treated mice or control mice were conducted into an under-agarose assay (21). Figure 2J shows that miR-451 overexpression decreased neutrophil migration toward fMLP. These data indicate that overexpression of miR-451 in neutrophils decreases chemotaxis to the site of inflammation.

MicroRNA-451 directly targets CPNE3 and Rab5a genes. MicroRNA-451 is known to suppress Rab14 (17), 14-3-3ζ (29,30), and CUGBP2 (31) directly. To investigate the role of miR-451 in neutrophils, we sought new target genes of miR-451. We generated a miR-451 expression vector, which up-regulated miR-451 expression by 8- and 15-fold, 24 hours (data not shown) and 48 hours (Figure 3A) after transfection, respectively.

Open-access software (including TargetScan [32] and miRanda [33]), which was used to screen for target genes that have complementary sites for miR-451 in their 3′-UTR, predicted >1,600 putative target genes. We selected 12 candidate genes that were expected to be involved in neutrophil function, and we inserted the 3′-UTR sequences of each candidate gene downstream of the firefly luciferase reporter gene of the pmirGLO

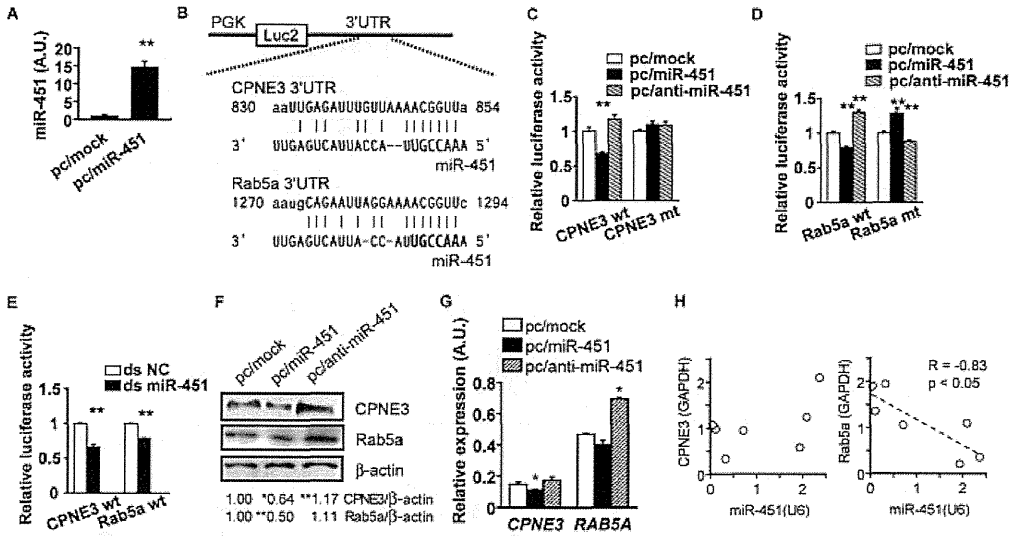

Figure 3. MicroRNA-451 (miR-451) directly targets CPNE3 and Rab5a genes. **A,** HeLa cells were transfected with pcDNA6.2/miR-mock (pc/mock) vector or pcDNA6.2/miR-451 (pc/miR-451) vector. Expression of miR-451 (normalized to U6 expression) in HeLa cells was measured by real-time quantitative polymerase chain reaction (qPCR) 48 hours after transfection (n = 6). **B,** The putative miR-451–binding sequence in the 3′-untranslated region (3′-UTR) of CPNE3 and RAB5a mRNA is shown. Human CPNE3 or Rab5a 3′-UTR fragments containing a wild-type (WT) or mutant (mt) miR-451–binding sequence were inserted downstream of the luciferase reporter gene. Seed sequences complementary to the target sequences are indicated in boldface. **C** and **D,** The wild-type or mutant reporter plasmid containing a 3′-UTR fragment of CPNE3 (**C**) or Rab5a (**D**) was cotransfected into HeLa cells with the pcDNA6.2/miR-mock, pcDNA6.2/miR-451, or pcDNA6.2/anti–miR-451 (pc/anti–miR-451) vectors (n = 6), and relative luciferase activity was measured. **E,** The wild-type reporter plasmid containing a 3′-UTR fragment of CPNE3 or Rab5a was cotransfected into HeLa cells with double-stranded miR-451 (ds-miR-451) or negative control (NC) siRNA (n = 3). **F** and **G,** HeLa cells were transfected with the pcDNA6.2/miR-mock, pcDNA6.2/miR-451, or pcDNA6.2/anti–miR-451 vectors. Expression of the CPNE3 and Rab5a proteins was analyzed by Western blot assay (**F**) (results shown are representative of 4 experiments), and expression of CPNE3 and Rab5a mRNA relative to GAPDH was analyzed by real-time qPCR (n = 6) (**G**). **H,** The correlation between the expression of miR-451 and the expression of CPNE3 or Rab5a in neutrophils from patients with rheumatoid arthritis (n = 7) was analyzed. The relative expression levels of miR-451, CPNE3, and Rab5a (normalized to the expression of U6 or GAPDH) are shown. Values in **A, C, D, E,** and **G** are the mean ± SEM. * = $P < 0.05$; ** = $P < 0.01$, versus pcDNA6.2/miR-mock in **A, C, D,** and **G** and versus controls in **E.**

vector. The pmirGLO vector and the miR-451–overexpressing vector, control vector, or anti–miR-451–overexpressing vector were cotransfected into HeLa cells, and luciferase activity was measured (Figures 3B–D).

Overexpression of miR-451 down-regulated luciferase activity with the target sequences of CPNE3 and Rab5a downstream of the firefly luciferase gene, while suppression of miR-451 up-regulated luciferase activity (Figures 3C and D). Although, luciferase with mutated 3′-UTR sequences of Rab5a was paradoxically influenced by the miR-451 vector, luciferase with mutated 3′-UTR sequences of CPNE3 was not influenced by overexpression or down-regulation of miR-451 as expected. Transfection of synthesized double-stranded miR-451 also decreased luciferase activity in each pmirGLO vector (Figure 3E). Overexpression of miR-451 also significantly down-regulated the expression of protein and mRNA for native CPNE3 and Rab5a in HeLa cells (Figures 3F and G). In contrast, down-regulation of miR-451 increased these expression levels (Figures 3F and G). These data suggest that miR-451 affects the expression of CPNE3 and Rab5a at both the transcriptional and translational levels.

Previous reports have detailed the expression of CPNE3 and Rab5a in human neutrophils (34,35). We also analyzed the expression of CPNE3 and Rab5a in neutrophils from RA patients and healthy controls, and there were no significant differences in expression (data not shown). However, the expression of Rab5a was negatively correlated with the expression of miR-451 in RA patients ($R = -0.83$, $P < 0.05$) (Figure 3H), indicating that Rab5a is regulated by miR-451 in RA neutrophils.

MicroRNA-451 down-regulates the p38 MAPK signaling pathway via 14-3-3ζ and Rab5a. During the host response to bacterial infection or tissue injury,

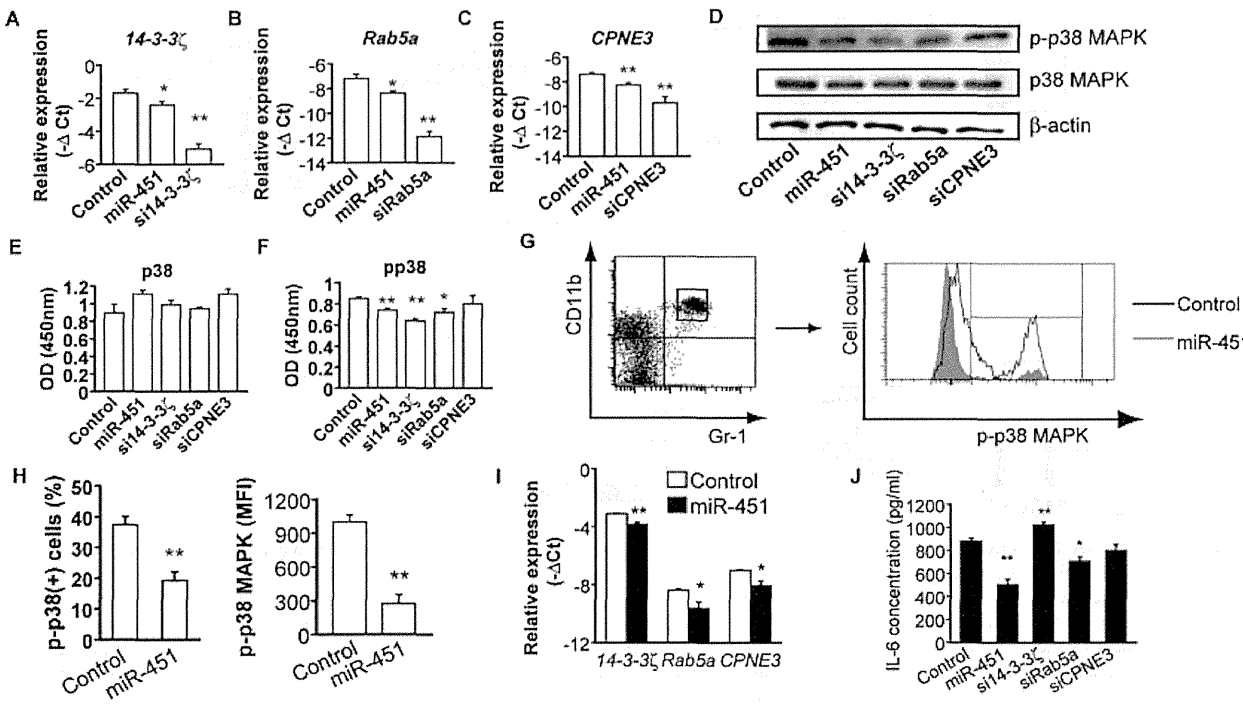

Figure 4. Overexpression of microRNA-451 (miR-451) inactivates the p38 MAPK signaling pathway via 14-3-3ζ and Rab5a. **A–C,** Expression of mRNA for 14-3-3ζ (**A**), Rab5a (**B**), and CPNE3 (**C**) relative to GAPDH in HeLa cells transfected with small interfering RNA (siRNA) (as a negative control), double-stranded miR-451, or siRNA for 14-3-3ζ, Rab5a, or CPNE3 (n = 6 experiments) was analyzed by real-time quantitative polymerase chain reaction (qPCR). **D,** Levels of p38 MAPK and phospho-p38 MAPK in whole-cell extracts from negative control siRNA, double-stranded miR-451, and siRNA-transfected 14-3-3ζ, Rab5a, or CPNE3 HeLa cells were assessed by Western blotting, with β-actin used as a control. Images are representative of 3 independent experiments. **E** and **F,** The amount of p38 MAPK (**E**) and phospho-p38 MAPK (**F**) was quantified by enzyme-linked immunosorbent assay (ELISA) (n = 6 experiments). **G,** Phospho-p38 MAPK in Gr-1+CD11b+ neutrophils was detected by flow cytometry. Neutrophils were harvested from spleens of mice 24 hours after intravenous administration of double-stranded miR-451 or control siRNA. **H,** The percentage of phospho-p38+ cells and the mean fluorescence intensity (MFI) of phospho-p38 MAPK were quantified (n = 5 mice per group). **I,** Expression of mRNA for 14-3-3ζ, Rab5a, and CPNE3 relative to GAPDH in fibroblast-like synoviocytes (FLS) 48 hours after transfection with negative control siRNA or double-stranded miR-451 (n = 4 experiments) was analyzed by real-time qPCR. **J,** After transfection with negative control siRNA, double-stranded miR-451, or siRNAs for 14-3-3ζ, Rab5a, and CPNE3 for 48 hours, FLS were cultured in serum-free Dulbecco's modified Eagle's medium with 10 ng/ml tumor necrosis factor α for 48 hours. The concentration of interleukin-6 (IL-6) in the conditioned medium was quantified by ELISA (n = 5). Values in **A–C**, **E**, **F**, and **H–J** are the mean ± SEM. * = $P < 0.05$; ** = $P < 0.01$ versus controls.

neutrophils respond to multiple chemoattractants. However, neutrophils must ultimately disengage from some chemoattractants and migrate unidirectionally toward the bacteria-derived chemoattractants (21). Neutrophils prioritize chemotactic signals by distinguishing "intermediary" (leukotriene B_4, CXCL8, and platelet-activating factor) and "end-target" (fMLP and C5a) chemoattractants through distinct intracellular signaling pathways. Although the phosphoinositide 3-kinase pathway is important in the intermediary chemoattractant pathway, p38 MAPK plays an important role in migration of neutrophils toward the end-target chemoattractant.

To evaluate the effect of miR-451 on p38 MAPK, we prepared siRNAs for Rab5a, CPNE3, and 14-3-3ζ (because 14-3-3ζ is thought to associate with p38 MAPK) (30). Messenger RNA for 14-3-3ζ, Rab5a, and CPNE3 was degraded when HeLa cells were transfected with siRNA for each gene (Figures 4A–C). Transfection of double-stranded miR-451 also significantly decreased 14-3-3ζ, Rab5a, and CPNE3 mRNA levels (Figures 4A–C).

Western blot analysis showed that the expression of p38 MAPK was not affected in cells transfected with double-stranded miR-451 or with siRNA for 14-3-3ζ, Rab5a, or CPNE3, whereas the phosphorylation of p38

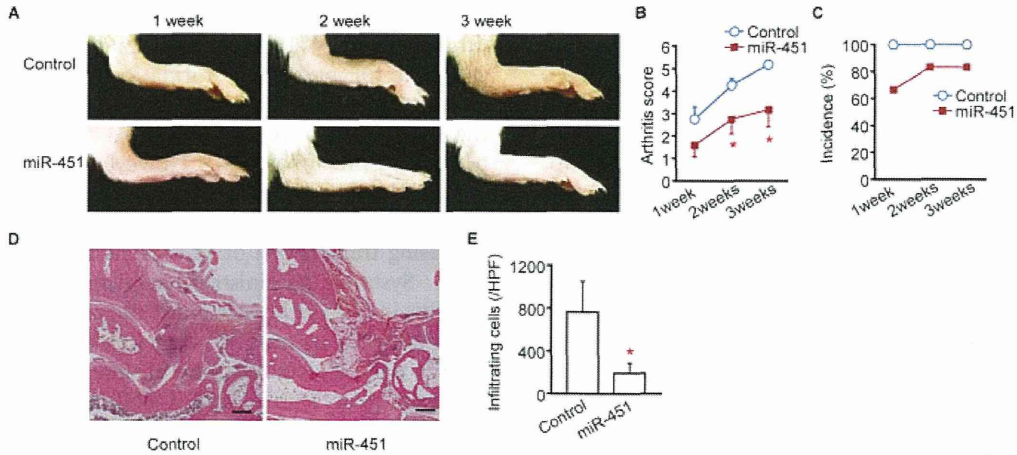

Figure 5. Administration of double-stranded microRNA-451 (miR-451) ameliorates autoimmune arthritis in SKG mice. Female SKG mice (8–12 weeks old) were injected intraperitoneally with 20 mg of mannan. Double-stranded miR-451 or control small interfering RNA (n = 6 mice per group) was administered intravenously on days 0, 4, 7, and 11. **A–C**, Representative joint swelling (**A**), mean ± SEM arthritis scores (**B**), and incidence of arthritis (**C**) in SKG mice at 1, 2, and 3 weeks after mannan treatment. **D,** Representative histologic findings in SKG mice 3 weeks after mannan treatment. Hematoxylin and eosin stained; bars = 200 μm. **E,** Number of cells infiltrating into the synovial tissue per high-power field (hpf) (n = 6 mice per group). Values are the mean ± SEM. $*$ = $P < 0.05$ versus controls.

MAPK was down-regulated (Figure 4D). The amount of p38 or phospho-p38 MAPK was quantified by ELISA (Figures 4E and F). Phospho-p38 MAPK content decreased in cells transfected with double-stranded miR-451, 14-3-3ζ siRNA, or Rab5a siRNA. These data suggest that up-regulation of miR-451 expression inhibited the phosphorylation of p38 MAPK via 14-3-3ζ and Rab5a but not CPNE3. No significant effect on the phosphorylation of Akt, a downstream molecule of the phosphoinositide 3-kinase pathway, was observed in cells transfected with double-stranded miR-451 (data not shown).

Next, we harvested neutrophils from the spleens of mice that had received double-stranded miR-451 or control siRNA intravenously. Flow cytometric analysis showed that miR-451 overexpression decreased phospho-p38 MAPK in Gr-1+CD11b+ neutrophils (Figures 4G and H). These data suggest that overexpression of miR-451 decreases phospho-p38 MAPK in murine neutrophils as well.

To further determine the role of miR-451 and its target genes, including Rab5a and CPNE3, we investigated IL-6 production in RA FLS. We confirmed that transfection of double-stranded miR-451 significantly decreased 14-3-3ζ, Rab5a, and CPNE3 mRNA levels, even in FLS from RA patients (Figure 4I). While transfection of 14-3-3ζ siRNA enhanced the production of IL-6 ($P < 0.01$), overexpression of miR-451 and knockdown of Rab5a or CPNE3 down-regulated the production of IL-6 ($P < 0.01$, $P < 0.05$, and $P = 0.09$, respectively) (Figure 4J), implying involvement of miR-451 in the pathogenesis of RA (including in the priming of neutrophils via IL-6) (36).

Administration of double-stranded miR-451 ameliorates autoimmune arthritis. We demonstrated that administration of miR-451 markedly decreased the infiltration of neutrophils in an air-pouch model. However, various types of immune cells are also involved in the pathogenesis of RA. SKG mice, which harbor a mutation of the gene encoding ZAP-70 on a BALB/c background, develop self-sustained arthritis after a single injection of mannan (37). To examine the involvement of miR-451 in the development of autoimmune arthritis, we injected double-stranded miR-451 intravenously twice a week into mannan-treated SKG mice.

Intravenous administration of miR-451 reduced the severity of arthritis significantly (Figures 5A and B) and reduced the incidence slightly (Figure 5C). Histologic analysis indicated that synovitis was suppressed and that the number of cells infiltrating the synovium was reduced significantly in mice treated with double-stranded miR-451 (Figures 5D and E). Attenuation of arthritis by administration of miR-451 suggests that down-regulation of miR-451 expression might lead to exacerbation of autoimmune arthritis partly by dysregulation of the chemotaxis of infiltrating cells. It also

indicates that administration of miR-451 is a potential treatment for RA.

DISCUSSION

MicroRNAs are of interest because of their critical role as fine regulators of gene expression at the posttranscriptional level within cells in many diseases, and because they are potential targets in the treatment of disease. The abnormal pattern of miRNA expression has been reported in various diseases, and the suppression of overexpressed miRNAs or reconstitution of the expression by restoration of silenced miRNAs is a therapeutic target in many fields (4).

MicroRNA-451 has been shown to play an important role in erythropoiesis (38) and in suppressing tumor growth by regulating cell proliferation and apoptosis (16,17). It has also been suggested that miR-451 contributes to CD4+ T cell function (39). Thus, we assumed that miR-451 was relevant to autoimmune arthritis and that reduced expression of miR-451 in neutrophils implied that miR-451 was possibly crucial to neutrophil function.

Transcriptional regulation of miR-451 is largely unknown; however, miR-451 was shown to be transcriptionally activated by transcription factor 3 in T cells (40). E2A activity is inhibited by a Ras/ERK/MAPK pathway (41), which is activated by GM-CSF stimulation (42). Early growth response 1, an inhibitory factor of transcription factor 3, is stimulated by IFNγ independently of STAT-1 (43). Stimulation with GM-CSF or IFNγ might down-regulate the expression of miR-451 in neutrophils via this pathway.

Neutrophil chemotaxis driven by the complement pathway has an important function in animal models of arthritis (44), and the possible contribution of neutrophils to RA pathology, even in the early phases, has been reported (1). Neutrophils are the first cell type to arrive at sites of inflammation. They secrete immune mediators that can activate neutrophils and other immune cells, triggering positive regulatory feedback that may lead to acute and persistent inflammation. Neutrophils live longer in inflammatory sites, where they augment the release of powerful destructive enzymes. These cells are also thought to be involved in bone remodeling and bone resorption through membrane-bound RANKL, which activates monocyte fusion into fully functional osteoclasts (45). Neutrophils can interact with other cells, such as antigen-presenting cells and osteoclast-like cells, and can regulate their function. Thus, neutrophils are considered to be more than simple final effectors.

Rab5a and CPNE3 are newly identified direct targets of miR-451. Rab5a is a small GTPase, and it is essential for endosome formation and trafficking in neutrophils and macrophages (46,47). CPNE3 exists in the cytosol of neutrophils and is expressed in immature neutrophil precursors (34). However, the true function of CPNE3 in neutrophils is unknown because the short lifespan of neutrophils limits the ability to investigate this using transfection or in vivo microinjection studies.

Systemic administration of miR-451 suppressed arthritis in SKG mice. Although the reduced chemotaxis of neutrophils by miR-451 explains this suppression at least in part, the contribution of other cells may also be assumed. Via Rab5a and CPNE3, miR-451 down-regulated the production of IL-6 from FLS, which play a fundamental role in driving the inflammation associated with RA at both the local and systemic levels. We also confirmed that miR-451 down-regulated the proliferation of FLS independent of Rab5a and CPNE3 (data not shown). A recent study demonstrated that inhibition of miR-451 in dendritic cells increased the production of IL-6, TNF, CCL3, CCL5, and IFNβ via 14-3-3ζ when cells were transfected with influenza (18). Proinflammatory mediators, including TNFα, IL-1β, and cyclooxygenase 2, are downstream of p38 MAPK (48). Systemic administration of miR-451 might relieve inflammation in autoimmune arthritis via these mechanisms.

The present study has a few limitations. It is difficult to deliver precursor miR-451 specifically to neutrophils. We confirmed that the expression of miR-451 in neutrophils from mice transfected with double-stranded miR-451 was 1.8 times as high as in neutrophils from control mice. However, surrounding cells, which were also transfected with miR-451, might prime the condition of neutrophils in vivo prior to isolation. More efficient direct methods to deliver miRNA are needed for the clinical use of small RNAs. Although we showed that miR-451 inhibits the phosphorylation of p38 MAPK via 14-3-3ζ and Rab5a, it remains to be determined how crucial these genes are for the regulation of p38 MAPK by miR-451.

Another limitation of this study is that we could not identify the function of CPNE3 in neutrophils, and we could not elucidate fully the mechanism by which miR-451 suppresses autoimmune arthritis. The function of CPNE3 in neutrophils and the role of miR-451 in other cells including T cells, B cells, and synovial cells should be investigated in the future. Nevertheless, this study shows for the first time the obvious suppressive function of miR-451 in neutrophil chemotaxis and in autoimmune arthritis.

In conclusion, we demonstrated that miR-451 suppressed neutrophil chemotaxis via p38 MAPK in vitro and in vivo and ameliorated autoimmune arthritis, and our analysis identified new direct targets of miR-451. These findings suggest that miR-451 is a potential target in the treatment of RA.

ACKNOWLEDGMENTS

We gratefully acknowledge the patients and volunteers who consented to blood collection for use in this study. We thank Koji Yamamoto, Motomu Hashimoto, Yoshinaga Ito, and Ryoko Nakanishi (Kyoto University) for their excellent help. We also thank Associate Professor Tomoki Aoyama (Kyoto University) for permission to use the Applied Biosystems 7500 Thermocycler for real-time quantitative polymerase chain reaction and the BD FACSCanto II.

AUTHOR CONTRIBUTIONS

All authors were involved in drafting the article or revising it critically for important intellectual content, and all authors approved the final version to be published. Dr. Yoshitomi had full access to all of the data in the study and takes responsibility for the integrity of the data and the accuracy of the data analysis.

Study conception and design. Murata, Yoshitomi.

Acquisition of data. Murata, Yoshitomi, Furu, Ishikawa, Shibuya, Ito.

Analysis and interpretation of data. Murata, Yoshitomi, Matsuda.

REFERENCES

1. Cascao R, Rosario HS, Souto-Carneiro MM, Fonseca JE. Neutrophils in rheumatoid arthritis: more than simple final effectors. Autoimmun Rev 2010;9:531–5.
2. Luo X, Tsai LM, Shen N, Yu D. Evidence for microRNA-mediated regulation in rheumatic diseases. Ann Rheum Dis 2010;69 Suppl 1:i30–6.
3. Kozomara A, Griffiths-Jones S. miRBase: integrating microRNA annotation and deep-sequencing data. Nucleic Acids Res 2011;39: D152–7.
4. Filkova M, Jungel A, Gay RE, Gay S. MicroRNAs in rheumatoid arthritis: potential role in diagnosis and therapy. BioDrugs 2012; 26:131–41.
5. Lewis BP, Burge CB, Bartel DP. Conserved seed pairing, often flanked by adenosines, indicates that thousands of human genes are microRNA targets. Cell 2005;120:15–20.
6. Stanczyk J, Leslie Pedrioli DM, Brentano F, Sanchez-Pernaute O, Kolling C, Gay RE, et al. Altered expression of microRNA in synovial fibroblasts and synovial tissue in rheumatoid arthritis. Arthritis Rheum 2008;58:1001–9.
7. Pauley KM, Satoh M, Chan AL, Bubb MR, Reeves WH, Chan EK. Upregulated miR-146a expression in peripheral blood mononuclear cells from rheumatoid arthritis patients. Arthritis Res Ther 2008;10:R101.
8. Niimoto T, Nakasa T, Ishikawa M, Okuhara A, Izumi B, Deie M, et al. MicroRNA-146a expresses in interleukin-17 producing T cells in rheumatoid arthritis patients. BMC Musculoskelet Disord 2010;11:209.
9. Stanczyk J, Ospelt C, Karouzakis E, Filer A, Raza K, Kolling C, et al. Altered expression of microRNA-203 in rheumatoid arthritis synovial fibroblasts and its role in fibroblast activation. Arthritis Rheum 2011;63:373–81.
10. Mitchell PS, Parkin RK, Kroh EM, Fritz BR, Wyman SK, Pogosova-Agadjanyan EL, et al. Circulating microRNAs as stable blood-based markers for cancer detection. Proc Natl Acad Sci U S A 2008;105:10513–8.
11. Murata K, Yoshitomi H, Tanida S, Ishikawa M, Nishitani K, Ito H, et al. Plasma and synovial fluid microRNAs as potential biomarkers of rheumatoid arthritis and osteoarthritis. Arthritis Res Ther 2010;12:R86.
12. Wang H, Peng W, Ouyang X, Li W, Dai Y. Circulating micro RNAs as candidate biomarkers in patients with systemic lupus erythematosus. Transl Res 2012;160:198–206.
13. Murata K, Furu M, Yoshitomi H, Ishikawa M, Shibuya H, Hashimoto M, et al. Comprehensive microRNA analysis identifies miR-24 and miR-125a-5p as plasma biomarkers for rheumatoid arthritis. PLoS One 2013;8:e69118.
14. Kirschner MB, Kao SC, Edelman JJ, Armstrong NJ, Vallely MP, van Zandwijk N, et al. Haemolysis during sample preparation alters microRNA content of plasma. PLoS One 2011;6:e24145.
15. Dore LC, Amigo JD, dos Santos CO, Zhang Z, Gai X, Tobias JW, et al. A GATA-1-regulated microRNA locus essential for erythropoiesis. Proc Natl Acad Sci U S A 2008;105:3333–8.
16. Nan Y, Han L, Zhang A, Wang G, Jia Z, Yang Y, et al. MiRNA-451 plays a role as tumor suppressor in human glioma cells. Brain Res 2010;1359:14–21.
17. Wang R, Wang ZX, Yang JS, Pan X, De W, Chen LB. MicroRNA-451 functions as a tumor suppressor in human non-small cell lung cancer by targeting ras-related protein 14 (RAB14). Oncogene 2011;30:2644-58.
18. Rosenberger CM, Podyminogin RL, Navarro G, Zhao GW, Askovich PS, Weiss MJ, et al. miR-451 regulates dendritic cell cytokine responses to influenza infection. J Immunol 2012;189: 5965–75.
19. Arnett FC, Edworthy SM, Bloch DA, McShane DJ, Fries JF, Cooper NS, et al. The American Rheumatism Association 1987 revised criteria for the classification of rheumatoid arthritis. Arthritis Rheum 1988;31:315–24.
20. Chalaris A, Rabe B, Paliga K, Lange H, Laskay T, Fielding CA, et al. Apoptosis is a natural stimulus of IL6R shedding and contributes to the proinflammatory trans-signaling function of neutrophils. Blood 2007;10:1748–55.
21. Heit B, Robbins SM, Downey CM, Guan Z, Colarusso P, Miller BJ, et al. PTEN functions to 'prioritize' chemotactic cues and prevent 'distraction' in migrating neutrophils. Nat Immunol 2008; 9:743–52.
22. Heit B, Tavener S, Raharjo E, Kubes P. An intracellular signaling hierarchy determines direction of migration in opposing chemotactic gradients. J Cell Biol 2002;159:91–102.
23. Du J, Chen L, Luo X, Shen Y, Dou Z, Shen J, et al. 14-3-3ζ cooperates with phosphorylated Plk1 and is required for correct cytokinesis. Front Biosci (Schol Ed) 2012;4:639–50.
24. Chen PI, Kong C, Su X, Stahl PD. Rab5 isoforms differentially regulate the trafficking and degradation of epidermal growth factor receptors. J Biol Chem 2009;284:30328–38.
25. Heinrich C, Keller C, Boulay A, Vecchi M, Bianchi M, Sack R, et al. Copine-III interacts with ErbB2 and promotes tumor cell migration. Oncogene 2010;29:1598–610.
26. Nishitani K, Ito H, Hiramitsu T, Tsutsumi R, Tanida S, Kitaori T, et al. PGE2 inhibits MMP expression by suppressing MKK4-JNK MAP kinase-c-JUN pathway via EP4 in human articular chondrocytes. J Cell Biochem 2010;109:425–33.
27. Hirota K, Yoshitomi H, Hashimoto M, Maeda S, Teradaira S, Sugimoto N, et al. Preferential recruitment of CCR6-expressing Th17 cells to inflamed joints via CCL20 in rheumatoid arthritis and its animal model. J Exp Med 2007;204:2803–12.
28. Kadl A, Galkina E, Leitinger N. Induction of CCR2-dependent macrophage accumulation by oxidized phospholipids in the air-pouch model of inflammation. Arthritis Rheum 2009;60:1362–71.
29. Yu D, dos Santos CO, Zhao G, Jiang J, Amigo JD, Khandros E,

et al. miR-451 protects against erythroid oxidant stress by repressing 14-3-3ζ. Genes Dev 2010;24:1620–33.
30. Zhang Z, Luo X, Ding S, Chen J, Chen T, Chen X, et al. MicroRNA-451 regulates p38 MAPK signaling by targeting of Ywhaz and suppresses the mesangial hypertrophy in early diabetic nephropathy. FEBS Lett 2012;586:20–6.
31. Wang X, Zhu H, Zhang X, Liu Y, Chen J, Medvedovic M, et al. Loss of the miR-144/451 cluster impairs ischaemic preconditioning-mediated cardioprotection by targeting Rac-1. Cardiovasc Res 2012;94:379–90.
32. TargetScan software: release 6.2. Cambridge (MA): Whitehead Institute for Biomedical Research; 2012. URL: http://www.targetscan.org/.
33. MiRanda at MicroRNA.org. Computational Biology Center, Memorial Sloan-Kettering Cancer Center. URL: http://www.microrna.org/.
34. Cowland JB, Carter D, Bjerregaard MD, Johnsen AH, Borregaard N, Lollike K. Tissue expression of copines and isolation of copines I and III from the cytosol of human neutrophils. J Leukoc Biol 2003;74:379–88.
35. Vita F, Soranzo MR, Borelli V, Bertoncin P, Zabucchi G. Subcellular localization of the small GTPase Rab5a in resting and stimulated human neutrophils. Exp Cell Res 1996;227:367–73.
36. Fielding CA, McLoughlin RM, McLeod L, Colmont CS, Najdovska M, Grail D, et al. IL-6 regulates neutrophil trafficking during acute inflammation via STAT3. J Immunol 2008;181:2189–95.
37. Hashimoto M, Hirota K, Yoshitomi H, Maeda S, Teradaira S, Akizuki S, et al. Complement drives Th17 cell differentiation and triggers autoimmune arthritis. J Exp Med 2010;207:1135–43.
38. Patrick DM, Zhang CC, Tao Y, Yao H, Qi X, Schwartz RJ, et al. Defective erythroid differentiation in miR-451 mutant mice mediated by 14-3-3ζ. Genes Dev 2010;24:1614–9.
39. Morandi F, Pistoia V. Soluble HLA-G modulates miRNA-210 and miRNA-451 expression in activated $CD4^+$ T lymphocytes. Int Immunol 2013;25:279–85.
40. Li X, Sanda T, Look AT, Novina CD, von Boehmer H. Repression of tumor suppressor miR-451 is essential for NOTCH1-induced oncogenesis in T-ALL. J Exp Med 2011;208:663–75.
41. Engel I, Murre C. The function of E- and Id proteins in lymphocyte development. Nat Rev Immunol 2001;1:193–9.
42. Lehman JA, Gomez-Cambronero J. Molecular crosstalk between p70S6k and MAPK cell signaling pathways. Biochem Biophys Res Commun 2002;93:463–9.
43. Ramana CV, Gil MP, Han Y, Ransohoff RM, Schreiber RD, Stark GR. Stat1-independent regulation of gene expression in response to IFN-γ. Proc Natl Acad Sci U S A 2001;98:6674–9.
44. Ji H, Ohmura K, Mahmood U, Lee DM, Hofhuis FM, Boackle SA, et al. Arthritis critically dependent on innate immune system players. Immunity 2002;16:157–68.
45. Poubelle PE, Chakravarti A, Fernandes MJ, Doiron K, Marceau AA. Differential expression of RANK, RANK-L, and osteoprotegerin by synovial fluid neutrophils from patients with rheumatoid arthritis and by healthy human blood neutrophils. Arthritis Res Ther 2007;9:R25.
46. Feliciano WD, Yoshida S, Straight SW, Swanson JA. Coordination of the Rab5 cycle on macropinosomes. Traffic 2011;12:1911–22.
47. McLaughlin NJ, Banerjee A, Khan SY, Lieber JL, Kelher MR, Gamboni-Robertson F, et al. Platelet-activating factor-mediated endosome formation causes membrane translocation of $p67^{phox}$ and $p40^{phox}$ that requires recruitment and activation of p38 MAPK, Rab5a, and phosphatidylinositol 3-kinase in human neutrophils. J Immunol 2008;180:8192–203.
48. Schieven GL. The biology of p38 kinase: a central role in inflammation. Curr Top Med Chem 2005;5:921–8.

ORIGINAL ARTICLE

JBMR®

Inhibition of miR-92a Enhances Fracture Healing via Promoting Angiogenesis in a Model of Stabilized Fracture in Young Mice

Koichi Murata,[1] Hiromu Ito,[1,2] Hiroyuki Yoshitomi,[1,3] Koji Yamamoto,[1] Akinobu Fukuda,[4] Junsuke Yoshikawa,[4] Moritoshi Furu,[1,2] Masahiro Ishikawa,[1] Hideyuki Shibuya,[1] and Shuichi Matsuda[1]

[1]Department of Orthopaedic Surgery, Kyoto University Graduate School of Medicine, Kyoto, Japan
[2]Department of the Control for Rheumatic Diseases, Kyoto University Graduate School of Medicine, Kyoto, Japan
[3]Center for Innovation in Immunoregulative Technology and Therapeutics, Kyoto University Graduate School of Medicine, Kyoto, Japan
[4]Department of Orthopaedic Surgery, Yoshikawa Hospital, Kyoto, Japan

ABSTRACT

MicroRNAs (miRNAs) are endogenous small noncoding RNAs regulating the activities of target mRNAs and cellular processes. Although no miRNA has been reported to play an important role in the regulation of fracture healing, several miRNAs control key elements in tissue repair processes such as inflammation, hypoxia response, angiogenesis, stem cell differentiation, osteogenesis, and chondrogenesis. We compared the plasma concentrations of 134 miRNAs in 4 patients with trochanteric fractures and 4 healthy controls (HCs), and the levels of six miRNAs were dysregulated. Among these miRNAs, miR-92a levels were significantly decreased 24 hours after fracture, compared to HCs. In patients with a trochanteric fracture or a lumbar compression fracture, the plasma concentrations of miR-92a were lower on days 7 and 14, but had recovered on day 21 after the surgery or injury. To determine whether systemic downregulation of miR-92a can modulate fracture healing, we administered antimir-92a, designed using locked nucleic acid technology to inhibit miR-92a, to mice with a femoral fracture. Systemic administration of antimir-92a twice a week increased the callus volume and enhanced fracture healing. Enhancement of fracture healing was also observed after local administration of antimir-92a. Neovascularization was increased in mice treated with antimir-92a. These results suggest that plasma miR-92a plays a crucial role in bone fracture healing in human and that inhibition of miR-92a enhances fracture healing through angiogenesis and has therapeutic potential for bone repair. © 2014 American Society for Bone and Mineral Research.

KEY WORDS: MICRORNA; FRACTURE HEALING; ANGIOGENESIS; LOCKED NUCLEIC ACID; BIOMARKER

Introduction

Fracture healing is a complex process orchestrated by a precise sequence of growth factors and cytokines that control activation, proliferation, and differentiation of local mesenchymal stem or progenitor cells. Under optimal conditions, a fractured bone heals without any scar formation and fully recovers its morphological and biomechanical properties. However, accelerated bone regeneration is required in demanding situations such as skeletal reconstruction of large bone defects created by trauma, infection, tumor resection, or skeletal abnormalities. The regenerative processes can be compromised in suboptimal situations such as avascular necrosis, atrophic nonunion, and catastrophic injury with impaired vasculature.[1]

Currently, various strategies are used to augment an impaired or insufficient bone-regeneration process, including distraction osteogenesis, bone transport, administration of growth factors, osteoconductive scaffolds, osteoprogenitor cells, and a number of bone-grafting methods.[1] Most of the current strategies for bone regeneration exhibit relatively satisfactory results, but there are some notable limitations to their effectiveness and availability. Overcoming the limitations of the current methods requires elucidation of bone healing mechanisms to produce more effective and accessible treatment modalities. These reparative processes comprise a variety of molecular and cellular events that recapitulate several aspects of skeletal development including vascularization and recruitment of mesenchymal stem cells,[2–4] but the precise mechanisms responsible for these processes have not been elucidated fully.

MicroRNAs (miRNAs) are endogenous, small, noncoding RNAs that mediate mRNA cleavage, translational repression, and mRNA destabilization. Currently more than 2200 human miRNAs are registered (miRBase Release 19).[5] miRNAs play diverse roles in fundamental biological processes such as cell proliferation, differentiation, growth, apoptosis, stress response, and tumorigenesis. miRNAs have been implicated in various aspects of

Received in original form February 9, 2013; revised form June 10, 2013; accepted June 24, 2013. Accepted manuscript online July 16, 2013.
Address correspondence to: Hiromu Ito, MD, PhD, Department of the Control for Rheumatic Diseases, Kyoto University Graduate School of Medicine, 54 Kawahara-cho, Shogoin, Sakyo, Kyoto 606-8507, Japan. E-mail: hiromu@kuhp.kyoto-u.ac.jp
Additional Supporting Information may be found in the online version of this article.

Journal of Bone and Mineral Research, Vol. 29, No. 2, February 2014, pp 316–326
DOI: 10.1002/jbmr.2040

embryonic development, such as neuronal, muscle, and cardiovascular organogenesis.[6,7] Increasing evidence suggests that miRNAs regulate chondrocyte, osteoblast, and osteoclast differentiation,[8–14] implying important roles in fracture repair. However, to date, no reports have been available regarding miRNAs that regulate fracture healing or treatment strategies using miRNAs to enhance fracture healing.

miRNAs are present in human plasma called as circulating miRNAs in a remarkably stable form, protected from endogenous RNase activity.[15] Altered expression of circulating miRNAs have been reported in patients with rheumatoid arthritis[16] and patients with cancer,[15,17,18] suggesting their usefulness as biomarkers and tools for analyzing the pathogenesis of disease or injury. Although circulating miRNAs are expected to be useful biomarkers of fractures or postoperative conditions, no biomarker has been evaluated as an indicator of a patient's condition after fracture or surgery.

In this study, we showed that plasma miR-92a concentrations in human significantly decreased after 24 hours following fracture, compared to healthy controls (HCs). Neovascularization and the bone healing processes were promoted by systemic and local inhibition of miR-92a using a locked nucleic acid (LNA)-stabilized oligonucleotide in a mouse femoral fracture model. These results suggest that plasma miR-92a plays a crucial role in bone fracture healing and that the inhibition of miR-92a has a therapeutic potential in enhancing bone repair.

Subjects and Methods

Preparation of blood samples

Ethical approval for this study was granted by the ethics committee of Kyoto University Graduate School and Faculty of Medicine. Informed consent was obtained from all participants. Plasma samples were obtained from 26 patients with a bone fracture when they first visited the hospital. Three patients with a trochanteric fracture and patients with a lumbar compression fracture provided plasma within 24 hours of injury and days 7, 14, and 21 after the surgery or injury. Blood was also collected from volunteer HCs who were not being treated for arthralgia, heart failure, renal failure, or an autoimmune disease. The backgrounds of the patients with a fracture and HCs are shown in Supplementary Table 1. Blood samples were collected with EDTA-2K–containing tubes to separate the plasma. Samples were centrifuged at 1400*g* for 7 minutes, and the plasma samples were stored at –80°C until analyzed.

Mouse rib and femoral fracture model

All animal studies were conducted in accordance with principles and procedures approved by Kyoto University Committee of Animal Resources, based on International Guiding Principles for Biomedical Research Involving Animals. A mouse rib or femoral fracture model was created using 6-week-old wild-type (C57BL/6NCrSlc) mice. Details for creating rib fracture models have been described.[19] The surgical protocol for producing a femoral fracture included a longitudinal incision and blunt separation of the underlying muscles with care not to remove the periosteum as described.[20] A transverse osteotomy in the mid-diaphysis of the femur was created with a low-speed rotary diamond disk with saline irrigation. The fractured bones were then repositioned and stabilized by inserting a 23-gauge intramedullary needle.

Total RNA isolation from cellular, tissue samples, and conditioned medium

Total RNA was extracted from cell samples using a High Pure miRNA Isolation Kit (Roche Applied Science, Mannheim, Germany) according to the manufacturer's protocol. For tissue samples, the samples were snap-frozen in liquid nitrogen, homogenized with TriPure Isolation Reagent (Roche Applied Science), incubated for 5 minutes at room temperature, mixed with 0.2 volume of chloroform, shaken vigorously for 15 seconds, incubated for 3 minutes, and centrifuged at 12,000*g* for 15 minutes at 4°C. Then 300 μL of the aqueous phase was applied to the High Pure miRNA Isolation Kit according to the manufacturer's protocol. Total RNA included in the conditioned medium or plasma was isolated as described.[16]

Quantitative real-time polymerase chain reaction of mature miRNAs

Reverse transcription was performed using NCode VILO miRNA cDNA Synthesis Kit (Life Technologies, Carlsbad, CA, USA) according to the manufacturer's protocol. Using EXPRESS SYBR GreenER qPCR SuperMix (Life Technologies), quantitative real-time polymerase chain reaction (qRT-PCR) was performed on an Applied Biosystems 7500 Thermocycler (Life Technologies) according to the manufacturer's protocol with standard plasmids generated as described[16] or with synthetic first-strand cDNAs with anticipated sequences. A total of 134 miRNAs were measured to screen for plasma biomarkers for bone fractures; the primer sequences for these miRNAs are listed in Supplementary Table 2. The data were analyzed using SDS Relative Quantification Software version 2.06 (Life Technologies). The miRNA expression data for the cellular and tissue samples from mice were normalized against small nuclear RNA MBII-202 (sno202). The absolute concentration of miRNAs in each liquid sample was calculated as described.[16]

Locked nucleic acid

Endotoxin-free antisense oligonucleotides were synthesized as hybrid molecules between deoxyribonucleotides and 2′-O-4′-O-methylene bridge (locked nucleic acid [LNA]) modification of all G and C residues with a complete phosphorothioate backbone by GeneDesign (Ibaraki, Japan). The sequences of the miR-92a inhibitor (antimir-92a) and its scrambled control are 5′-CAGGCCGGGACAAGTGCAATA-3′ and 5′-GCATCAAGACGGTCAGAGCGA-3′, as described.[21] LNA was administered intravenously into the tail vein (75 μg/75 μL) on days 0, 4, 7, 11, and 14 after the surgery, or locally around the fracture site (25 μg/100 μL) on days 4, 7, 11, and 14 after the fracture.

Radiographic analysis of fracture callus formation

Bone radiographs were taken with a soft X-ray instrument (CMB-2; SOFTEX, Ebina, Japan). Radiographic images were scored as follows: 1, no apparent hard callus; 2, slight intramembranous ossification; 3, hard callus without bridging of the fracture gap, fracture line is apparent; 4, hard callus with bridging of the fracture gap, fracture gap is noticeable; 5, unclear boundary between the newly formed hard callus and existing cortical bone; and 6, remodeling. Radiographic images were evaluated independently by two experienced orthopedic surgeons (KM, MI), and when the interpretations differed, the score was decided after discussion with KM, MI, and HI. Fractured femurs were scanned using an TDM1000 micro–computed tomography (μCT)

system (Yamato Scientific, Tokyo, Japan) at 1024 views, 16 frames per view, 60 kV, and 60 μA. The callus volume of interest for a fractured bone was determined with TRI/3D-BON64 software (Ratoc System Engineering, Tokyo, Japan). Callus volume was calculated using TRI/3D-BON64 software. We scanned a set of hydroxyapatite (HA) phantoms and defined our mineralization threshold as 300 mg HA/cm^3.

μCT analysis of neovascularization of the fracture sites

Vascularity of the fracture callus was evaluated using a μCT-based method.[22–24] Briefly, the entire vascular system was flushed by injecting heparinized (100 units/mL) normal saline, and then a radioopaque, lead chromate-based contrast agent (Flow Tech, Carver, MA, USA) was perfused by intracardiac injection. After perfusion, animals were kept at 4°C for 24 hours to allow the compound to polymerize. The femora were stored at 4°C for 48 hours in 4% paraformaldehyde, soaked for 21 days in 10% ethylenediaminetetraacetic acid (EDTA) solution for decalcification, washed thoroughly using water, and placed in 4% paraformaldehyde until imaging. Specimens were scanned using SMX-100CT-SV-3 (Shimadzu, Kyoto, Japan) at 2400 views, 5 frames per view, 37 kV, and 121 μA. Three-dimensional images of the radioopaque contrast-filled vascular network were rendered and evaluated using VGStudio MAX (Nihon Visual Science Software, Tokyo, Japan).

Histological analysis

Decalcified specimens were processed to obtain paraffin-embedded sections with a thickness of 5 to 7 μm, and the sections were stained with hematoxylin and eosin (HE) and HE/Alcian blue. Immunohistochemical staining was performed as described.[25] Specimens were incubated with rabbit anti-CD31 antibodies (Abcam, Cambridge, MA, USA; 1:50 dilution) overnight at 4°C. The number of CD31-positive vessels was counted in randomly selected areas around the fracture callus. The number of blood vessels was counted in the HE-stained sections. Cross-sectional vessel area was measured with ImageJ software (National Institutes of Health, Bethesda, MD, USA) as described.[26]

Luciferase assay

We inserted a 3′-untranslated region (3′UTR) fragment containing putative binding sites for miR-92a into the NheI-SalI fragment of the pmirGLO vector (Promega, Fitchburg, WI, USA). The sequences of inserted oligonucleotides are shown in Supplementary Table 3.

We transfected C3H10T1/2 cells with the luciferase reporter vector and double-stranded miR-92a (miCENTURY OX miNatural; Cosmo Bio, Tokyo, Japan) or the nonspecific negative control siRNA with using X-tremeGENE siRNA Transfection Reagent (Roche Applied Science). Luciferase activity was measured 24 hours after transfection using the Dual-Luciferase Reporter Assay System (Promega) according to the manufacturer's instructions.

Primary osteoblast isolation, cell line, and transfection

Primary osteoblasts were harvested from calvaria of newborn mice by sequential collagenase digestion (Roche Applied Science) and were seeded at a density of 2.5×10^4 cells/cm^2 maintained in α modified essential medium (α-MEM) containing 10% fetal bovine serum (FBS) as described.[27]

Antimir-92a or control LNA (final concentration of 150 nM) was transfected using Lipofectamine 2000 (Life Technologies) when the primary osteoblasts reached 70% confluency, and cells were maintained for 14 days with the differentiation medium supplemented with 10 mM β-glycerophosphate (Wako, Osaka, Japan), 80 mg/mL ascorbic acid phosphate (Wako), and with 10^{-8} M dexamethasone (Nacalai Tesque, Kyoto, Japan) as described.[28] The culture medium was replaced every second day. Alkaline phosphatase (ALP) staining of primary osteoblasts was performed as described,[28] and ALP activity was also evaluated with the tartrate-resistant acid phosphatase (TRACP) and ALP Assay Kit (Takara Bio, Otsu, Japan), according to the manufacturer's instructions.

MC3T3-E1 or ATDC5 cells were seeded at a density of 1×10^4 cells/cm^2 or 2×10^4 cells/cm^2 18 hours before transfection and transfected using Lipofectamine 2000 (Life Technologies), according to the manufacturer's protocol. The MC3T3-E1 cells were maintained in α-MEM containing osteogenic supplements including, 10% FBS, 10 mM β-glycerophosphate, and 50 μg/mL of ascorbic acid,[29] and ATDC5 cells were grown and maintained in DMEM and F12 at a 1:1 ratio with 5% FBS supplemented with insulin (10 μg/mL) (Sigma, St. Louis, MO, USA), transferrin (5.5 μg/mL) (Sigma), and sodium selenite (5 ng/mL) (Sigma) to induce chondrocyte differentiation, as described.[30]

qRT-PCR of mRNA

Reverse transcription was performed using a Transcriptor High Fidelity cDNA Synthesis Kit (Roche Applied Science) according to the manufacturer's protocol. Using FastStart Universal SYBR Green Master (Roche Applied Science), qRT-PCR was carried out on an Applied Biosystems 7500 thermocycler according to the manufacturer's protocol. The primer sequences are listed in Supplementary Table 4. All gene expression data were normalized against glyceraldehyde-3-phosphate dehydrogenase.

Statistical analysis

The data are presented as the mean ± SEM, unless otherwise noted. The radiographic scores were analyzed using the Mann-Whitney *U* test. Differences between three groups were analyzed with the Bonferroni method. Unless otherwise noted, Student's *t* test was used for statistical analysis; $p < 0.05$ was considered significant.

Results

Plasma miR-92a levels were decreased 24 hours after fracture

miRNAs are present in human plasma in a stable form despite the endogenous RNase activity, called circulating miRNA and are known as noninvasive biomarkers for detection of cancer[15,17,18,31] and of rheumatoid arthritis.[16] To determine whether plasma miRNA concentrations are changed in fracture-healing processes, we quantified the plasma levels of 134 randomly selected miRNAs in 4 patients with a trochanteric fracture and in 4 HCs and compared the average levels of each miRNA between the fracture and the HC group (Fig. 1*A*). Six miRNAs were identified with a more than a twofold differential expression ($p < 0.05$) between patients with a trochanteric fracture and HCs (Fig. 1*B*).

We next measured the concentration of these six miRNAs in 26 patients with a bone fracture and 26 HCs (data not shown).

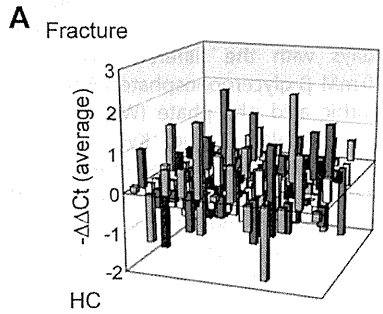

B

	median (- Δ Ct)		ΔΔCt	fold change	P value
	Fracture	HC			
miR-16	-2.7	-1.1	-1.6	2.9	0.01
miR-19b-1	-9.0	-7.8	-1.2	2.3	0.05
miR-25	-2.8	-1.6	-1.2	2.2	0.01
miR-92a	-1.9	-0.5	-1.4	2.7	0.01
miR-101	-6.6	-5.2	-1.4	2.6	0.01
miR-129-5p	-5.0	-4.0	-1.0	2.0	0.03

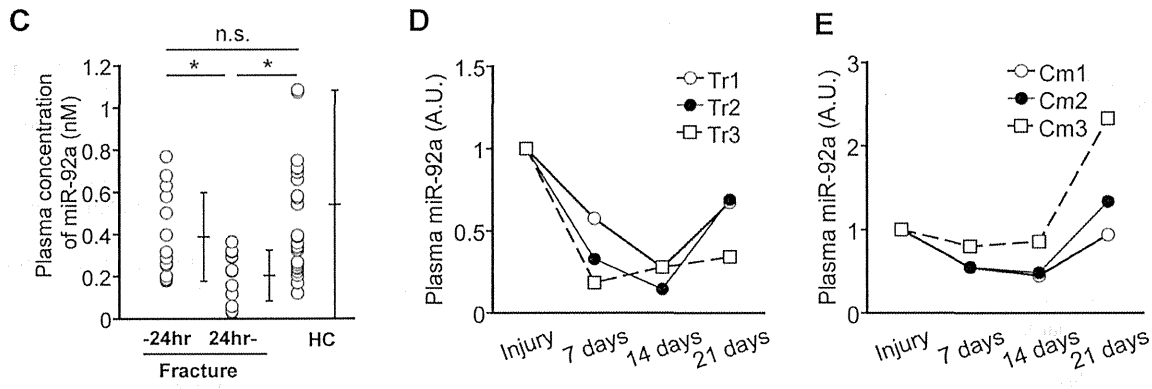

Fig. 1. Plasma concentrations of miRNAs in patients with a bone fracture. (*A*) Plasma concentrations of 134 miRNAs were compared between patients with a trochanteric fracture and HCs ($n = 4$ for each group). The averages of the differences in the Ct values between each miRNA and spike-in cel-miR-39 (−ΔCt) were calculated in each group, and the differences of the −ΔCt averages of each miRNA (−ΔΔCt) are demonstrated in the *z* axis. (*B*) Plasma miRNAs with more than a twofold differential expression with statistically significant difference ($p < 0.05$) between patients with a trochanteric fracture and HCs. (*C*) Plasma concentration of miR-92a in HCs ($n = 26$) and fracture patients within 24 hours of injury ($n = 14$) and 24 hours after injury ($n = 12$). The data are shown as mean ± SD. $^*p < 0.05$. (*D*) Plasma concentrations of miR-92a in 3 patients with a trochanteric fracture within 24 hours of injury and on postoperative days 7, 14, and 21. The data were normalized against the concentration at the time of the injury. (*E*) Plasma concentrations of miR-92a in 3 patients with a lumbar compression fracture within 24 hours of injury, and 7, 14, and 21 days after injury. The data were normalized against the concentration at the time of the injury. HC = healthy control; Ct = cycle threshold.

Among these miRNAs, only plasma miR-92a showed changes in concentration in association with fracture healing. Plasma miR-92a levels remained normal within the first 24 hours following fracture, and then significantly decreased compared to HCs (Fig. 1*C*), whereas there was no significant difference in the concentration when the fractured patients were analyzed altogether ($p = 0.09$). We also isolated blood from 3 patients with a trochanteric fracture and patients with a lumbar compression fracture within 24 hours of injury and 7, 14, and 21 days after the surgery or injury. Plasma miR-92a concentration was lower on days 7 and 14, and appeared to recover to the normal level by 21 days after the surgery or injury (Fig. 1*D*, *E*). These results suggest that plasma miR-92a has the potential to be a biomarker of, and may play an important role in, fracture healing.

Antimir knockdown of miR-92a enhanced endochondral bone formation in fracture healing of the femur

To identify the role of miR-92a in fracture healing, we intravenously introduced either an LNA-stabilized oligonucleotide that is antisense to miR-92a (antimir-92a) or a scrambled control into mice with a femoral fracture. We first analyzed the expression of miR-92a by qRT-PCR in fractured callus of the rib and the expression of miR-92a was not changed on postoperative days 2, 7, and 14 (Supplementary Fig. 1A). Second, qRT-PCR analysis showed successful knockdown of miR-92a in the femurs 24 and 48 hours after the intravenous injection of antimir-92a in mice without a fracture (Supplementary Fig. 1B).

Next, we radiographically evaluated the time course of endochondral bone formation in femoral fracture healing (Fig. 2*A*). Hard callus with bridging of the fracture gap was observed, and the fracture gap was noticeable on postfracture day 14 in both the control and antimir-92a groups; however, the callus volume was moderately larger in the antimir-92a group than in the control group. On postfracture day 21 in the control group, the callus volume became larger than on postfracture day 14, and the boundary between the newly formed hard callus and the existing cortical bone was about to diminish. By contrast, in the antimir-92a group, the boundary had disappeared and remodeling processes were observed, indicating accelerated bone repair. Bone formation in X-ray images was assessed using a radiographic score as described in Subjects and Methods, and a significant difference between the control group and antimir-92a group was observed on postfracture day 21 (Fig. 2*B*).

The callus volume was quantified by μCT. Total volume and bone volume of the callus was 84% and 45% larger in the antimir-92a group than in the control group on postfracture

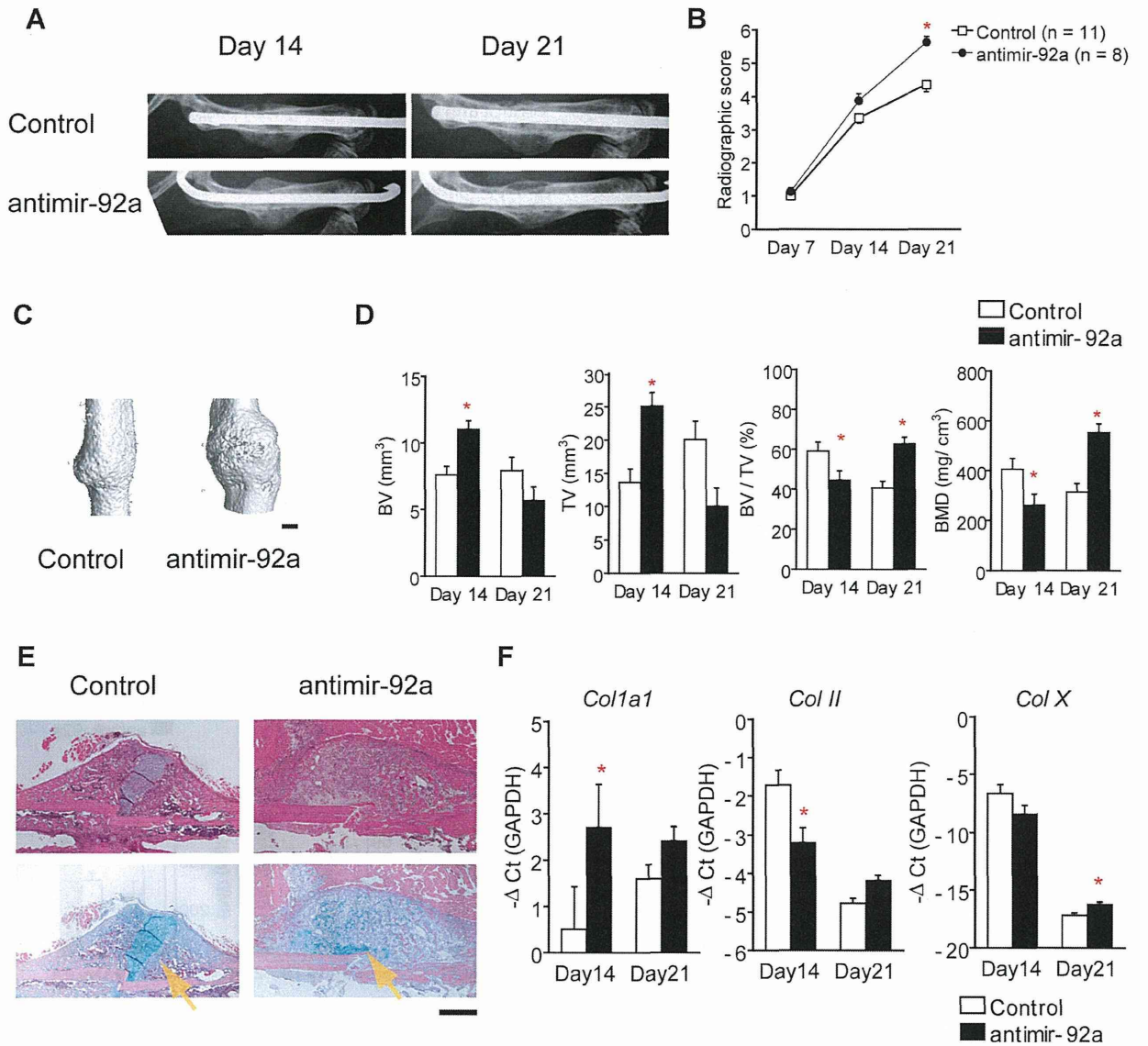

Fig. 2. Inhibition of miR-92a enhanced endochondral bone formation in mice with a femoral fracture. An LNA-stabilized oligonucleotide that is antisense to miR-92a (antimir-92a) or a scrambled control into mice with a femoral fracture intravenously on days 0, 4, 7, 11, and 14 after the surgery. (*A*) Time-dependent radiological changes in the femur, 14 and 21 days after the fracture. Representative images are shown. (*B*) Bone formation in X-ray images was assessed using a radiographic score as described in Subjects and Methods. (*C*) Representative 3D μCT image of a fractured femur on postoperative day 14. Scale bar = 1 mm. (*D*) TV and BV of the callus, BV/TV, and BMD on postoperative day 14 and 21 was quantified using μCT. $n = 6$ mice per group. (*E*) Histology of the fracture callus stained by HE or HE/Alcian-blue staining 14 days after the femoral fracture. Arrows indicate Alcian-blue–positive cartilage. (*F*) The expression levels of *Col1a1*, *Col II*, and *Col X* of callus from mice on postoperative day 14 and 21 were quantified by qRT-PCR ($n = 5$, respectively). Scale bar = 500 μm. The data are shown as mean ± SEM. $^*p < 0.05$. LNA = locked nucleic acid; 3D = three-dimensional; μCT = micro–computed tomography; TV = total volume; BV = bone volume; BMD = bone mineral density; HE = hematoxylin and eosin; qRT-PCR = quantitative real-time polymerase chain reaction.

day 14 (Fig. 2*C*, D). Because the remodeling processes had already occurred in the antimir-92a group, total volume or bone volume of the callus volume did not differ significantly between groups on postfracture day 21. Bone mineral density (BMD) was lower in the antimir-92a group on postfracture day 14. However, BMD significantly increased in the antimir-92a group compared with that in the control group.

Histological analyses on postfracture day 14 showed there was a larger area of cartilage at the fracture junction in the control group, indicating accelerated remodeling in the antimir-92a group (Fig. 2*E*).

Total RNA was extracted from callus on postfracture days 14 and 21. The expression of *Col1a* was significantly increased in the antimir-92a group compared to the control group on

postfracture day 14, and the difference in *Col1a* expression became smaller on postfracture day 21 (Fig. 2*F*). The expression of *Col II* and Col *X* was lower in the antimir-92a group than in the control group on postfracture day 14 and the downregulated expressions of *Col II* and *Col X* by antimir-92a were diminished on postfracture day 21. These data also support the accelerated bone healing in the antimir-92a group.

Local administration of antimir-92a enhanced endochondral bone formation in fracture healing of the femur

In clinical situations, the dosage of LNA and the possible side effects of an anti-miRNA (antimir) are of concern. Intraperitoneal injection of LNA is reportedly effective for the knockdown of miRNA.[32] Thus, we administered antimir-92a locally to the fracture site to examine whether local administration can induce an equivalent effect of antimir to that of systemic induction.

X-ray showed hard callus with a fracture gap in both the control and antimir-92a groups on postfracture day 14 (Fig. 3*A*). The callus volume was larger and the fracture gap was diminishing in the antimir-92a group compared with the control group. On postfracture day 21, the boundary between the newly formed hard callus and the existing cortical bone had disappeared and remodeling processes were observed in the antimir-92a group but not in the control group; these results were similar to those found in the samples after systemic administration. A higher score on bone formation in X-ray was

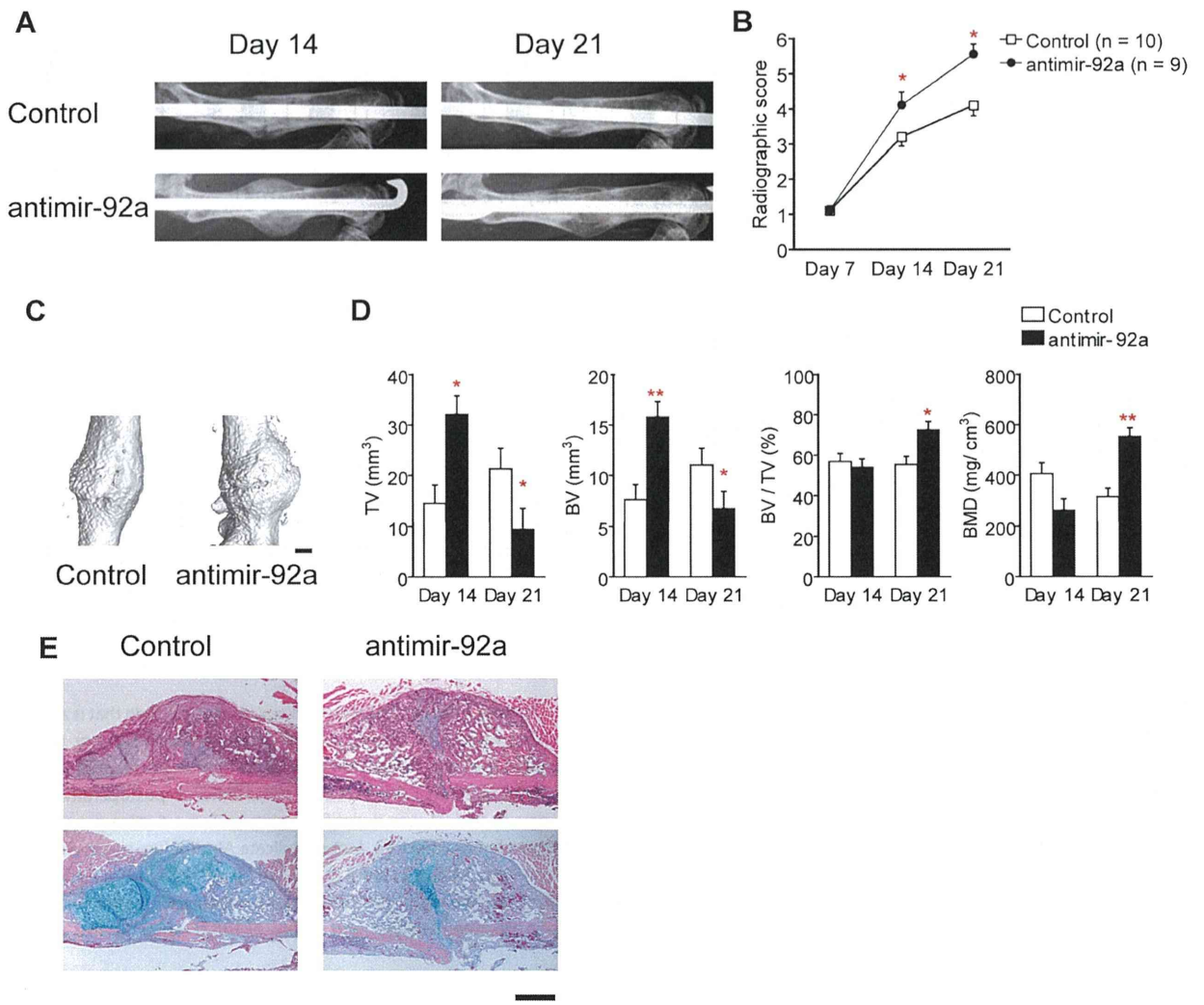

Fig. 3. Local administration of antimir-92a enhanced endochondral bone formation in fractured femora in mice. antimir-92a or a scrambled control was administered locally around the fracture site on days 4, 7, 11, and 14 after the fracture. (*A*) Time-dependent radiological changes in femurs 14 and 21 days after fracture. (*B*) Bone formation in the X-ray images was assessed by the radiographic score. (*C*) Representative 3D μCT images of a fractured femur on postoperative day 14. Scale bar = 1 mm. (*D*) TV and BV of the callus, BV/TV, and BMD on postoperative day 14 and 21 were quantified using μCT. $n = 5$–10 mice per group. (*E*) Histology of the fracture callus stained with HE or HE/Alcian blue staining 14 days after the femur fracture. Scale bar = 500 μm. The data are shown as mean ± SEM. $^{*}p < 0.05$; $^{**}p < 0.01$. 3D = three-dimensional; μCT = micro–computed tomography; TV = total volume; BV = bone volume; BMD = bone mineral density; HE = hematoxylin and eosin.

observed on postfracture days 14 and 21 between the control group and the antimir-92a group, similar to that observed for systemic administration (Fig. 3*B*).

Total volume and bone volume of the callus analyzed by μCT was 122% and 107%, respectively, larger in the antimir-92a group than in the control group on postfracture day 14 (Fig. 3*C*, *D*). No significant differences in total volume and bone volume of the callus were observed between the groups on postfracture day 21. There was no significant difference in BMD on postoperative day 14. However, BMD on postoperative day 21 in the antimir-92a group was significantly higher than in the control group.

Histological analysis on postfracture day 14 showed a greater proportion of mineralized tissues and a smaller proportion of the cartilage area in the antimir-92a group (Fig. 3*E*) compared with the control group. These findings indicate an accelerated healing in the antimir-92a group.

Inhibition of miR-92a did not affect osteoblast or chondrocyte differentiation

To examine the roles of miR-92a in osteoblast and chondrocyte differentiation, we tried to find new target genes of miR-92a, which should be highly expressed in osteoblasts or chondrocytes, by a computational screening for genes with complementary sites for miR-92a in their 3′UTR using open access software including TargetScan and miRanda. More than 4000 putative target genes were estimated, and miRanda identified alpha-2 type I collagen (Col1a2) and angiopoietin1 (ANGPT1) as potential targets of miR-92a. We conducted a luciferase reporter assay by cloning the 3′UTR of a putative target gene downstream of the firefly luciferase reporter gene in the pmirGLO vector and cotransfected these vectors with double-stranded miR-92a or mimics into C3H10T1/2. The luciferase activities were not downregulated (Supplementary Fig. 2), indicating that these genes were not direct targets of miR-92a.

Next, to analyze the effects of antimir-92a on osteoblast and chondrocyte differentiation, we isolated primary osteoblasts from neonatal calvariae. We transfected primary osteoblasts with antimir-92a and incubated the cells in differentiation medium for 14 days. The expression of *Runx2*, *Osterix*, *Osteocalcin*, *Col1a1*, and *ALP* did not differ between the control and the antimir-92a groups (Fig. 4*A*). ALP staining for the culture did not show a difference and there was no significant difference in ALP activity of the culture between the control and the antimir-92a groups (Fig. 4*B*), indicating no acceleration or deceleration of osteoblast differentiation by antimir-92a.

We also transfected MC3T3-E1 with antimir-92a and incubated the cells in differentiation medium for 2 days. The expression of *Osteocalcin* did not differ between the control and the antimir-92a groups (data not shown).

Similarly, no significant differences in the expression of *type II collagen (Col II)*, *type X collagen (Col X)*, and *Sox9* were observed in ATDC5 cells transfected with antimir-92a (Fig. 4*C*), indicating again no effect of miR-92a inhibition on chondrocyte differentiation.

These results suggest that antimir-92a did not affect either of osteoblast and chondrocyte differentiation.

Suppression of miR-92a enhanced angiogenesis during fracture healing

Because miR-92a has been shown to inhibit vascular development by targeting ITGA5,[33] we used μCT imaging of contrast-perfused, decalcified specimens to evaluate vascular growth within the fracture callus of mice (Fig. 5*A*). The vessel volume was 90% larger 14 days after surgery in the fracture callus of mice intravenously administered antimir-92a compared with those treated with scrambled control (Fig. 5*B*).

We also used immunohistochemistry to analyze the tissues surrounding the femoral fracture callus 14 days after surgery. The number of total and CD31-positive blood vessels increased 174% and 106%, respectively, in the antimir-92a group compared with the control group (Fig. 5*C*, *D*). The ratio of the vessel areas was also 300% higher in the antimir-92a group than in the control group.

Immunohistochemical staining analysis showed increased CD31-positive capillary invaded into the cartilage 14 days after surgery by the intravenous administration of antimir-92a (Fig. 5*E*). In accordance with the results above, the expression levels of *VEGF-A* and *ANGPT1* in fractured callus 14 days after surgery were significantly higher in the antimiR-92a group (Fig. 5*F*), suggesting that antimir-92a stimulates the angiogenesis in fractured callus and surrounding tissues. There was no significant difference in mRNA expression level of *ITGA5*, a known target of miR-92a, in fractured callus between the antimir-92a and the control group. Capillary invasion to the fractured callus by antimir-92a coincide with the results from microCT analysis, where no significant increase in BMD on postfracture day 14 was observed (Fig. 2*D*) and quick invasion might remain the Alcian blue-positive chondrocytes observed in the center of the callus (Fig. 2*E*).

Taken together, miR-92a plays a crucial role in inhibition of neovascularization in bone repair processes and that inhibition of miR-92a enhances fracture healing. Systemic and local administration of antimir are both effective for the enhancement of fracture repair.

Discussion

miRNAs have been shown to exist in a stable form in plasma despite endogenous RNase activity and are thought to have potential noninvasive biomarkers for detection of cancer[15,17,18,31] and of tissue injury.[34,35] However, no biomarker is currently available for evaluation of fracture healing in humans. Plasma miR-92a concentration was lower in fracture patients 24 hours after injury than in HCs and remained low 7 and 14 days after injury, suggesting that it can potentially indicate the status of fracture healing. Furthermore, the results suggest that miR-92a plays a crucial role in fracture healing. Although we cannot exclude the possibility that down-regulation of miR-92a reflects the response to inflammation or tissue injury, previous studies and the present data collectively indicate that changes of plasma miR-92a concentration show the status of neovascularization after a fracture. Indeed, there are both clinical and preclinical studies that show that markers of angiogenesis define both the progression of fracture healing and may be prognostic of delayed or failed bone healing.[36,37] Further analyses using a larger number of samples, including age-matched controls with various injuries, are needed.

miR-92a is encoded in the miR-17-92 cluster, which is highly expressed in human endothelial cells. The miR-17-92 cluster is essential for vertebrate development, because universal disruption of *Mirn17* in mice results in smaller embryos and immediate postnatal death. This is due to severely hypoplastic lungs and ventricular septal defects in the hearts of mice lacking

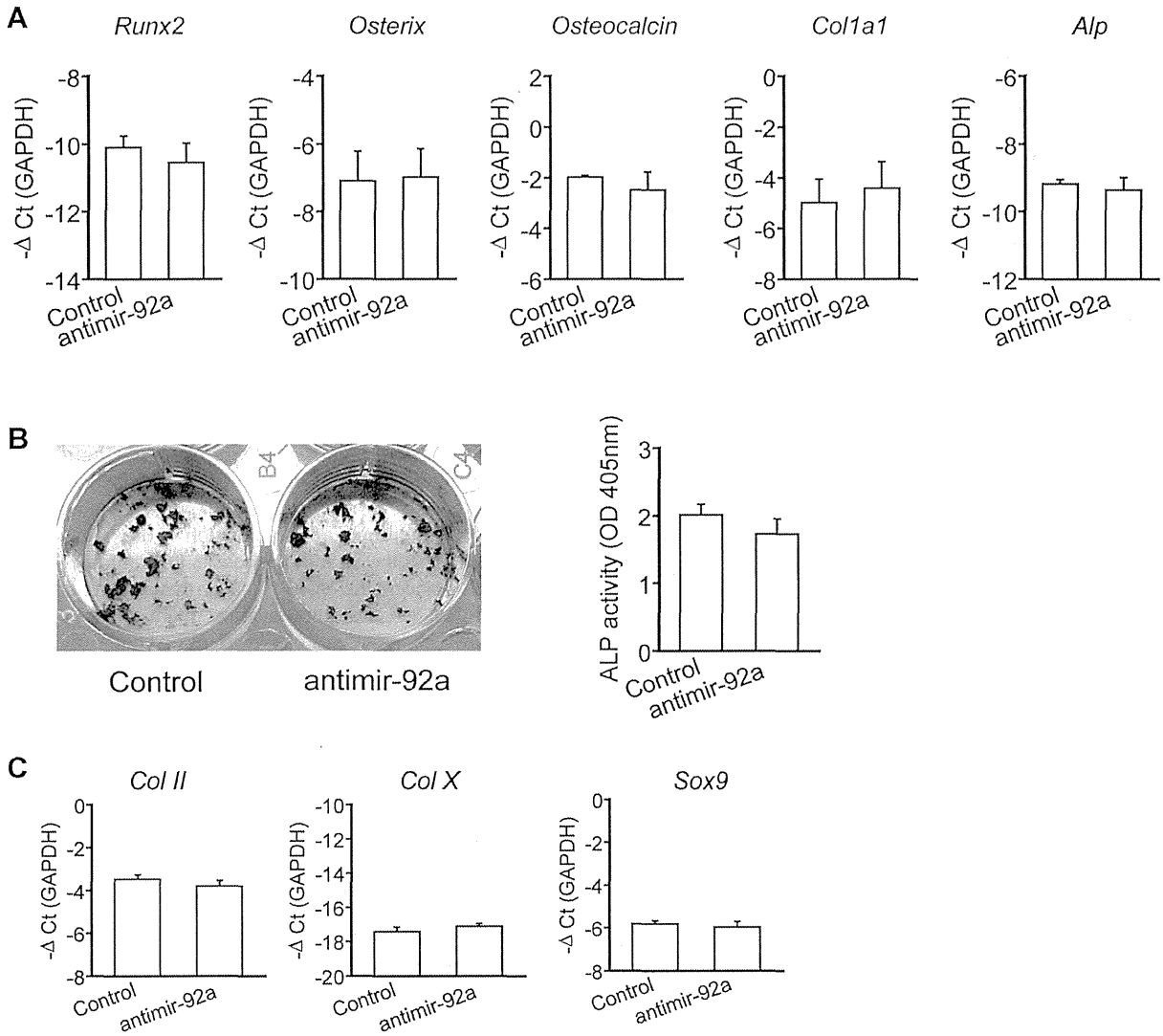

Fig. 4. Effects of miR-92a inhibition on osteoblast and chondrocyte differentiation. Primary osteoblasts were isolated from neonatal calvariae and transfected with antimir-92a or control LNA and incubated in differentiation medium for 14 days. (*A*) Total RNA was extracted, and the expression of each gene was analyzed by qRT-PCR ($n = 5$, respectively). (*B*) ALP activity was measured by ALP staining (representatives are shown) and ALP assay kit ($n = 8$, respectively). (*C*) ATDC5 cells were transfected with antimir-92a or control LNA and incubated in differentiation medium for 48 hours. Total RNA was extracted, and the expression of each gene was analyzed by qRT-PCR. ($n = 6$, respectively). The data are shown as mean ± SEM. $^*p < 0.05$. LNA = locked nucleic acid; qRT-PCR = quantitative real-time polymerase chain reaction; ALP = alkaline phosphatase; Ct = cycle threshold; OD = optical density.

miR-17-92.[38] These miRNAs are normally highly expressed in embryonic lung and decrease as mice reach maturity. Recently, haploinsufficiency of the miR-17-92 cluster was shown to impair skeletal bone formation as well as osteoblast proliferation and differentiation.[39] However, suppression of miR-92a was not sufficient in their mice and individual functions of miRNAs in the miR-17-92a cluster in osteoblasts have not been fully investigated.

miR-92a targets ITGA5 and MKK4[33,40] and is considered to inhibit angiogenesis. Angiogenesis is obviously important for bone fracture healing, because new blood vessels bring oxygen and nutrients to the highly metabolically active regenerating callus and serve as a route for inflammatory cells and mesenchymal progenitor cells to reach the injury site.[40] Defective angiogenesis at a fracture site can cause poor outcomes, including nonunion of the fracture, a clinical diagnosis made when a patient has clinical symptoms of pain at the fracture site, a pathological instability, and radiographic findings of unfused bone. We show here for the first time that miR-92a plays an essential role in bone healing in a mouse fracture model. Our results indicate that miR-92a inhibits neovascularization during the fracture healing processes. The possible reasons and mechanisms for the downregulation of plasma miR-92a remain to be investigated, but our study showed clearly that the inhibition of miR-92a can enhance neovascularization in a fracture model.

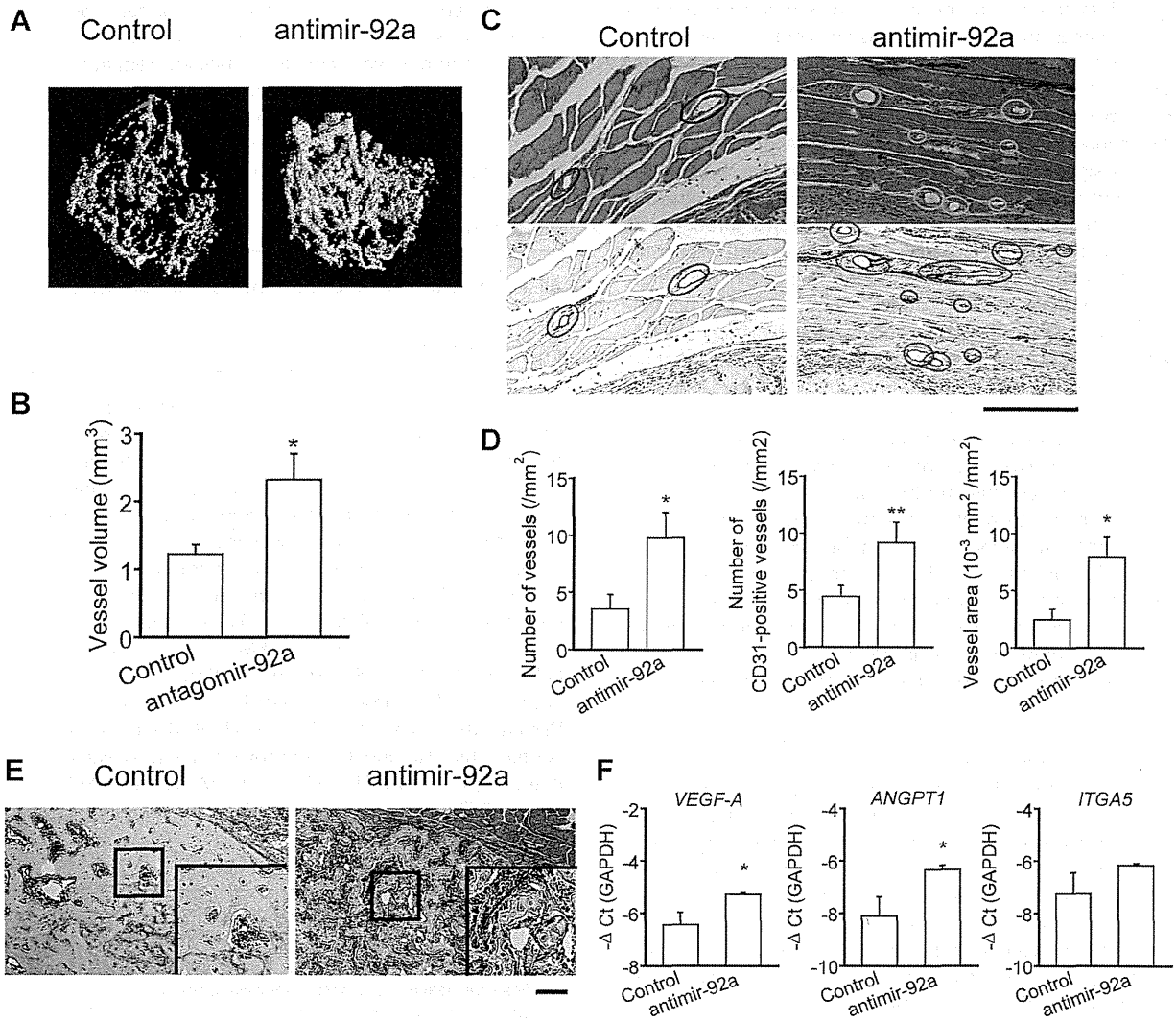

Fig. 5. Suppression of miR-92a enhanced angiogenesis during fracture healing. (*A*) Vascularity in the fractured femora of mice was visualized by μCT using a radioopaque silicon polymer medium on postfracture day 14. LNA was administered intravenously on days 0, 4, 7, 11, and 14 after the fracture. Representative images are shown. (*B*) On day 14 after surgery, vessel volume was quantified on 3D μCT images. $n = 5$–6 mice per group. The data are shown as mean ± SEM. $^*p < 0.05$. (*C*) Tissues surrounding the fracture callus on day 14 after surgery were stained with HE (upper panels) or stained immunohistochemically with anti-CD31 (lower panels). Scale bar = 200 μm. (*D*) The number of vessels in HE-stained samples (left panel) and CD31-positive vessels (middle panel) were counted, and the ratio of vessel area was measured in HE-stained samples (right panel) ($n = 5$–7 per group). (*E*) The fractured callus on postoperative day 14 were stained with anti-CD31 (lower panels). Representatives are shown and boxed areas are enlarged on right bottom. Scale bar for original images = 200 μm. (*F*) The expression levels of *VEGF-A*, *ANGPT1*, and *ITGA5* of callus from mice on postoperative day 14 were quantified by qRT-PCR ($n = 5$, respectively). The data are shown as mean ± SEM. $^*p < 0.05$; $^{**}p < 0.01$. LNA = locked nucleic acid; 3D = three-dimensional; μCT = micro–computed tomography; HE = hematoxylin and eosin; Ct = cycle threshold.

A possible concern would be that antagonizing a factor expressing in "normal fracture" may inhibit a normal repair process. However, this study demonstrated that an inhibitory factor for angiogenesis, miR-92a, is downregulated in normal fracture healing, and that even more downregulation of miR-92a accelerates fracture healing. Our hypothesis is that antiangiogenic factor(s) suppress unnecessary angiogenesis in normal conditions, but, once a tissue is injured, the factor(s) are suppressed, and neovascularization occurs. If one can inhibit those factors more effectively, the repair process would be accelerated. Side effects of the proangiogenic strategy are of concern, but any side effects were not found in this study. The proangiogenic therapeutic strategy has great possibilities for the future in accelerating fracture healing.

Various growth factors in the angiogenic cascade, including vascular endothelial growth factor, fibroblast growth factor, and platelet-derived growth factor, are potential targets for upregulation and direct administration to accelerate bone repair.[41] However, there are no reports describing an miRNA-based approach in treating bone fracture. miRNAs are considered to be

an attractive target for therapeutic manipulation, compared with the growth factors, due to the fact that one miRNA can regulate dozens of genes and can thus act as an amplifier. miRNAs are relatively stable small molecules whose expression levels can be manipulated by a growing number of technologies. To inhibit specific miRNAs, as shown in this study, oligonucleotides complementary to either the mature miRNA or its precursors can be designed such that the miRNA will be functionally arrested and will be unable to bind to the target mRNA subset.[42]

Plasma miRNAs are secreted in various form through cell-derived microvesicles including microparticles and exosomes, complexes with proteins including Ago2 protein and high-density lipoproteins, and apoptotic bodies.[43–46] The possible functions and protective mechanisms of circulating miRNAs remain unclear, but these forms of miRNAs can transfer a gene-silencing signal between living cells in vitro and in vivo, and they are considered to be used as cell-to-cell communication. Therefore, we systemically introduced LNA-stabilized antimir in mice with a femoral fracture, and the systemic induction strategy was proved to be effective for bone fracture healing.

The LNA-antimir technology adopted in this study has been used in miRNA inhibition experiments in vivo, and a phase II clinical trial is ongoing for SPC3649, an LNA-based antisense molecule against miR-122 for the treatment of hepatitis C.[32,47] In our study, successful downregulation was achieved even in the mouse femur (Supplementary Fig. 1B), suggesting that this LNA-based antisense therapy has unique potential in the treatment of bone injuries or disorders. Further modification to provide more effective transfer would enable this technology to be useful in therapeutic strategies in human diseases.

There are concerns that therapeutically induced angiogenesis may increase the risk of developing hemangioma, recurrence of malignant tumors, or deterioration of diabetic retinopathy.[48] Although we could not identify any side effects of antimir treatment given systemically or locally in this study, ensuring tissue-specific delivery and cellular uptake of sufficient amounts of synthetic oligonucleotide is a major challenge in the use of miRNA therapeutics in vivo and has been studied extensively.[49,50] In our study, local administration of an antimir was associated with bone fracture healing similar to that induced by systemic administration, suggesting that a lower dosage of an antimir can be administered locally yet produce similarly successful bone healing with potentially fewer side effects compared with systemic administration.

The present study has a few limitations. First, the dosage and interval of administration of antimir-92a was not optimized. A previous study showed that silencing of miR-122 and subsequent reduction in plasma cholesterol level could be achieved with 3 mg/kg of LNA,[32] and we adopted this dosage. It remains unclear when inhibition of miR-92a is necessary during the growth of new blood vessels, or when angiogenesis should be induced to enhance fracture healing. Additionally, local administration of an antimir may impair the healing of surrounding tissue unless it is administered at an appropriate time and in an appropriate volume. Optimization of the dosage, volume, timing, and delivery methods to an injured tissue is necessary.

Another limitation of this study is that the number of human samples was not sufficient for judging miR-92a as a useful biomarker. Patients with various bone fractures were included in this study, and HCs were younger than were patients with fractures. Samples from patients with a bone bruise may be appropriate as an optimal control group. Moreover, a longitudinal study with a sufficient sample size is mandatory for assessing the time-dependent changes in various fractures and injuries. Further analyses using a larger number of samples including age-matched controls with various injuries are required. However, this study shows, for the first time, that the plasma miRNA concentrations are downregulated during fracture healing.

In conclusion, inhibition of miR-92a by antimir enhanced bone healing in a mouse fracture model by promoting angiogenesis.

Disclosures

All authors state that they have no conflicts of interest.

Acknowledgments

This work was supported by a grant-in-aid from the Ministry of Education of Japan (No. 21591942, 23659719) and a grant from the Japan Orthopaedics and Traumatology Foundation, Inc. (Grant No. 262). The authors are grateful to all patients and volunteers who kindly provided blood for use in this study. We thank the staff at Yoshikawa Hospital for collecting the blood samples. We also thank Dr. Tomoki Aoyama, Dr. Toshiyuki Kitaori, and Ryoko Nakanishi (Kyoto University Graduate School of Medicine) for their valuable technical assistance.

Authors' roles: Study design. KM, HI, and KY. Study conduct: KM, HI, HY, KY, AF, JY, FM, MI, and HS. Data collection: KM, HI, KY, HS, and MI. Data interpretation: KM, HI, KY, MI, HY, and SM. Drafting the manuscript: KM and HI. Revising the manuscript content: KM, HI, and HY. Approving the final version of the manuscript: KM, HI, HY, MF, AF, JY, MI, HS, and SM. HI takes responsibility for the integrity of the data analysis.

References

1. Dimitriou R, Jones E, McGonagle D, Giannoudis PV. Bone regeneration: current concepts and future directions. BMC Med. 2011;9:66.
2. Gerstenfeld LC, Cullinane DM, Barnes GL, Graves DT, Einhorn TA. Fracture healing as a post-natal developmental process: molecular, spatial, and temporal aspects of its regulation. J Cell Biochem. 2003;88(5):873–4.
3. Kitaori T, Ito H, Schwarz EM, et al. Stromal cell-derived factor 1/CXCR4 signaling is critical for the recruitment of mesenchymal stem cells to the fracture site during skeletal repair in a mouse model. Arthritis Rheum. 2009;60(3):813–23.
4. Ito H, Koefoed M, Tiyapatanaputi P, et al. Remodeling of cortical bone allografts mediated by adherent rAAV-RANKL and VEGF gene therapy. Nat Med. 2005;11(3):291–7.
5. Kozomara A, Griffiths-Jones S. miRBase: integrating microRNA annotation and deep-sequencing data. Nucleic Acids Res. 2011;39: D152–7.
6. Kloosterman WP, Plasterk RH. The diverse functions of microRNAs in animal development and disease. Dev Cell. 2006; 11(4):441–50.
7. Stefani G, Slack FJ. Small non-coding RNAs in animal development. Nat Rev Mol Cell Biol. 2008;9(3):219–30.
8. Dong S, Yang B, Guo H, Kang F. MicroRNAs regulate osteogenesis and chondrogenesis. Biochem Biophys Res Commun. 2012;418(4): 587–91.
9. Kapinas K, Delany AM. MicroRNA biogenesis and regulation of bone remodeling. Arthritis Res Ther. 2011;13(3):220.
10. Wang X, Guo B, Li Q, et al. miR-214 targets ATF4 to inhibit bone formation. Nat Med. 2013;19(1):93–100.
11. Hu R, Liu W, Li H, et al. A Runx2/miR-3960/miR-2861 regulatory feedback loop during mouse osteoblast differentiation. J Biol Chem. 2011;286(14):12328–39.

12. Li H, Xie H, Liu W, et al. A novel microRNA targeting HDAC5 regulates osteoblast differentiation in mice and contributes to primary osteoporosis in humans. J Clin Invest. 2009;119(12):3666–77.
13. Lin EA, Kong L, Bai XH, Luan Y, Liu CJ. miR-199a, a bone morphogenic protein 2-responsive MicroRNA, regulates chondrogenesis via direct targeting to Smad1. J Biol Chem. 2009;284(17):11326–35.
14. Xu J, Kang Y, Liao WM, Yu L. MiR-194 regulates chondrogenic differentiation of human adipose-derived stem cells by targeting Sox5. PLoS One. 2012;7(3):e31861.
15. Mitchell PS, Parkin RK, Kroh EM, et al. Circulating microRNAs as stable blood-based markers for cancer detection. Proc Natl Acad Sci U S A. 2008;105(30):10513–8.
16. Murata K, Yoshitomi H, Tanida S, et al. Plasma and synovial fluid microRNAs as potential biomarkers of rheumatoid arthritis and osteoarthritis. Arthritis Res Ther. 2010;12:R86.
17. Schrauder MG, Strick R, Schulz-Wendtland R, et al. Circulating micro-RNAs as potential blood-based markers for early stage breast cancer detection. PLoS One. 2012;7(1):e29770.
18. Miyachi M, Tsuchiya K, Yoshida H, et al. Circulating muscle-specific microRNA, miR-206, as a potential diagnostic marker for rhabdomyosarcoma. Biochem Biophys Res Commun. 2010;400(1):89–93.
19. Ito H, Akiyama H, Shigeno C, Iyama K, Matsuoka H, Nakamura T. Hedgehog signaling molecules in bone marrow cells at the initial stage of fracture repair. Biochem Biophys Res Commun. 1999;262(2):443–51.
20. Matsubara H, Hogan DE, Morgan EF, Mortlock DP, Einhorn TA, Gerstenfeld LC. Vascular tissues are a primary source of BMP2 expression during bone formation induced by distraction osteogenesis. Bone. 2012;51(1):168–80.
21. Matsubara H, Takeuchi T, Nishikawa E, et al. Apoptosis induction by antisense oligonucleotides against miR-17-5p and miR-20a in lung cancers overexpressing miR-17-92. Oncogene. 2007;26(41):6099–105.
22. Xie C, Liang B, Xue M, et al. Rescue of impaired fracture healing in COX-2-/- mice via activation of prostaglandin E2 receptor subtype 4. Am J Pathol. 2009;175(2):772–85.
23. Duvall CL, Taylor WR, Weiss D, Wojtowicz AM, Guldberg RE. Impaired angiogenesis, early callus formation, and late stage remodeling in fracture healing of osteopontin-deficient mice. J Bone Miner Res. 2007;22(2):286–97.
24. Bouxsein ML, Boyd SK, Christiansen BA, Guldberg RE, Jepsen KJ, Muller R. Guidelines for assessment of bone microstructure in rodents using micro-computed tomography. J Bone Miner Res. 2010;25(7):1468–86.
25. Ishikawa M, Ito H, Akiyoshi M, et al. Lectin-like oxidized low-density lipoprotein receptor 1 signal is a potent biomarker and therapeutic target for human rheumatoid arthritis. Arthritis Rheum. 2012;64(4):1024–34.
26. O E, Lee BH, Ahn HY, et al. Efficient nonadhesive ex vivo expansion of early endothelial progenitor cells derived from CD34+ human cord blood fraction for effective therapeutic vascularization. FASEB J. 2011;25(1):159–69.
27. Kimura H, Kwan KM, Zhang Z, et al. Cthrc1 is a positive regulator of osteoblastic bone formation. PLoS One. 2008;3(9):e3174.
28. Nishio K, Neo M, Akiyama H, Okada Y, Kokubo T, Nakamura T. Effects of apatite and wollastonite containing glass-ceramic powder and two types of alumina powder in composites on osteoblastic differentiation of bone marrow cells. J Biomed Mater Res. 2001;55(2):164–76.
29. Li Z, Hassan MQ, Jafferji M, et al. Biological functions of miR-29b contribute to positive regulation of osteoblast differentiation. J Biol Chem. 2009;284(23):15676–84.
30. Murata K, Kitaori T, Oishi S, et al. Stromal cell-derived factor 1 regulates the actin organization of chondrocytes and chondrocyte hypertrophy. PLoS One. 2012;7(5):e37163.
31. Liu H, Zhu L, Liu B, et al. Genome-wide microRNA profiles identify miR-378 as a serum biomarker for early detection of gastric cancer. Cancer Lett. 2012;316(2):196–203.
32. Elmen J, Lindow M, Schutz S, et al. LNA-mediated microRNA silencing in non-human primates. Nature. 2008;452(7189):896–9.
33. Bonauer A, Carmona G, Iwasaki M, et al. MicroRNA-92a controls angiogenesis and functional recovery of ischemic tissues in mice. Science. 2009;324(5935):1710–3.
34. Long G, Wang F, Duan Q, et al. Circulating miR-30a, miR-195 and let-7b associated with acute myocardial infarction. PLoS One. 2012;7(12):e50926.
35. Bai Y, Wang L, Sun L, Ye P, Hui R. Circulating microRNA-26a: potential predictors and therapeutic targets for non-hypertensive intracerebral hemorrhage. Med Hypotheses. 2011;77(4):488–90.
36. Henle P, Zimmermann G, Weiss S. Matrix metalloproteinases and failed fracture healing. Bone. 2005;37(6):791–8.
37. Wigner NA, Kulkarni N, Yakavonis M, et al. Urine matrix metalloproteinases (MMPs) as biomarkers for the progression of fracture healing. Injury. 2012;43(3):274–8.
38. Ventura A, Young AG, Winslow MM, et al. Targeted deletion reveals essential and overlapping functions of the miR-17 through 92 family of miRNA clusters. Cell. 2008;132(5):875–86.
39. Zhou M, Ma J, Chen S, Chen X, Yu X. MicroRNA-17-92 cluster regulates osteoblast proliferation and differentiation. Endocrine. Epub. 2013 May 15. DOI:10.1007/s12020-013-9986-y
40. Lai L, Song Y, Liu Y, et al. MicroRNA-92a negatively regulates Toll-like receptor (TLR)-triggered inflammatory response in macrophages by targeting MKK4 kinase. J Biol Chem. 2013;288(11):7956–67.
41. Hankenson KD, Dishowitz M, Gray C, Schenker M. Angiogenesis in bone regeneration. Injury. 2011;42(6):556–61.
42. Roy S, Sen CK. miRNA in wound inflammation and angiogenesis. Microcirculation. 2012;19(3):224–32.
43. Arroyo JD, Chevillet JR, Kroh EM, et al. Argonaute2 complexes carry a population of circulating microRNAs independent of vesicles in human plasma. Proc Natl Acad Sci U S A. 2011;108(12):5003–8.
44. Kosaka N, Iguchi H, Yoshioka Y, Hagiwara K, Takeshita F, Ochiya T. Competitive interactions of cancer cells and normal cells via secretory microRNAs. J Biol Chem. 2012;287(2):1397–405.
45. Valadi H, Ekstrom K, Bossios A, Sjostrand M, Lee JJ, Lotvall JO. Exosome-mediated transfer of mRNAs and microRNAs is a novel mechanism of genetic exchange between cells. Nat Cell Biol. 2007;9(6):654–9.
46. Vickers KC, Palmisano BT, Shoucri BM, Shamburek RD, Remaley AT. MicroRNAs are transported in plasma and delivered to recipient cells by high-density lipoproteins. Nat Cell Biol. 2011;13(4):423–33.
47. Lanford RE, Hildebrandt-Eriksen ES, Petri A, et al. Therapeutic silencing of microRNA-122 in primates with chronic hepatitis C virus infection. Science. 2010;327(5962):198–201.
48. Keramaris NC, Calori GM, Nikolaou VS, Schemitsch EH, Giannoudis PV. Fracture vascularity and bone healing: a systematic review of the role of VEGF. Injury. 2008;39(Suppl 2):S45–57.
49. Zhang G, Guo B, Wu H, et al. A delivery system targeting bone formation surfaces to facilitate RNAi-based anabolic therapy. Nat Med. 2012;18(2):307–14.
50. Caporali A, Emanueli C. MicroRNA regulation in angiogenesis. Vascul Pharmacol. 2011;55(4):79–86.

Malrotated Tibial Component Increases Medial Collateral Ligament Tension in Total Knee Arthroplasty

Shinichi Kuriyama, Masahiro Ishikawa, Moritoshi Furu, Hiromu Ito, Shuichi Matsuda

Department of Orthopaedic Surgery, Graduate School of Medicine, Kyoto University, 54 Kawahara-cho, Shogoin, Sakyo-ku, Kyoto 606-8507, Japan

Received 26 December 2013; accepted 10 July 2014
Published online 29 August 2014 in Wiley Online Library (wileyonlinelibrary.com). DOI 10.1002/jor.22711

SUMMARY: Malrotation of the tibial component can lead to complications after total knee arthroplasty (TKA). Despite reports of internal rotation being associated with more severe pain or stiffness than external rotation, the biomechanical reasons remain largely unknown. We used a computer simulation model and evaluated traction forces in the lateral collateral ligament (LCL) and medial collateral ligament (MCL) with a malrotated tibial component during squatting. We also examined tibiofemoral and patellofemoral contact forces and stresses under similar conditions. A dynamic musculoskeletal knee model was simulated in three different constrained tibial geometries with a prototype component. The testing conditions were changed between 15° external and 15° internal rotation of the tibial component. With internal rotation of the tibial component, the MCL force increased progressively; the LCL force also increased, but only up to less than half of the MCL force values. A higher degree of constraint of the tibial component was associated with greater femoral rotational movement and higher MCL forces. The tibiofemoral and patellofemoral contact forces were not influenced by malrotation of the tibial component, but the contact stresses increased because of decreased contact area. This altered loading condition could cause patient complaints and polyethylene problems after TKA. © 2014 Orthopaedic Research Society. Published by Wiley Periodicals, Inc. J Orthop Res 32:1658–1666, 2014.

Keywords: total knee arthroplasty; medial collateral ligament; tibial component; malrotation; computer simulation

Proper positioning of the components is critical for ensuring a good clinical outcome of total knee arthroplasty (TKA). Surgeons focus on rotational alignment because correct rotational alignment is related to better function, clinical score, and range of motion after TKA. Excessive malposition of the tibial component, especially internal rotation, can lead to complications such as a painful knee,[1,2] a stiff knee,[3] patellofemoral instability,[4–6] or excessive polyethylene wear in the tibial component.[7] Accurate rotational placement of the tibial component is difficult to achieve freehand. Landmarks for rotational alignment are ambiguous compared with femoral rotational alignment, because the method of defining the tibial AP axis is variable.[8,9] Previous studies showed that internal rotational errors in the tibial component can be >20° in conventional TKA.[2,5] Even if a navigation system is used, the variation from the ideal rotational angle is larger for tibial than for femoral alignment.[10,11]

The etiology of knee joint pain or stiffness with a malrotated tibial component is unclear and may result from increased tension or pressure on soft tissue because of altered kinematics. Despite reports that internal rotation is associated with more severe pain or stiffness than external rotation, the biomechanical reasons remain largely unknown. We suppose that the symptoms associated with a malrotated tibial component could be affected by its surface geometry.

We used a musculoskeletal computer model to analyze three different constrained geometries for the tibial polyethylene insert during simulated weight-bearing deep knee flexion under quadriceps control. We evaluated the traction forces in the lateral collateral ligament (LCL) and medial collateral ligament (MCL) with a malrotated tibial component during squatting. We also examined whether tibiofemoral or patellofemoral contact forces and stresses increase under malrotated conditions.

MATERIALS AND METHODS

We used a dynamic musculoskeletal modeling program of the knee (LifeMOD/KneeSIM 2010; LifeModeler Inc., San Clemente, CA) that included tibiofemoral and patellofemoral contact, LCL, MCL, posterior cruciate ligament (PCL), elements of the knee capsule, quadriceps muscle and tendon, patellar tendon, and hamstring muscles. The LCL was considered a single fiber bundle; the MCL was considered as anterior and posterior bundles.[12–15] All ligament bundles were modeled as nonlinear springs with material properties obtained from a published report.[16] The ligaments were simulated as nonlinear force elements with their parabolic and linear equations as follows: if $\varepsilon < 0$, $F(\varepsilon) = 0$; if $0 \le \varepsilon \le 2\varepsilon_1$, $F(\varepsilon) = 0.25\,k\varepsilon^2/0.03$; and if $\varepsilon > 2\varepsilon_1$, $F(\varepsilon) = k\,(\varepsilon - 0.03)$, where F is the tension of the ligament, ε is the ligament strain, and k is the stiffness coefficient of each ligament. The linear range threshold was specified as $\varepsilon_1 = 0.03$. The hip joint was modeled as a revolute joint parallel to the flexion axis of the knee and was allowed to slide vertically. The ankle joint was modeled as a combination of several joints that combine to allow free translation in the ML direction and free rotation in the flexion, axial, and varus–valgus directions.

We adjusted the origins of the insertion points, stiffness, and length patterns of each ligament from the literature.[13,17–19] The LCL and MCL proximal attachment points were defined as the most prominent points of the femoral epicondyles. The LCL and MCL distal attachment points were adjusted to the tip of the fibular head and the midpoint

Grant sponsor: Adaptable and Seamless Technology Transfer Program through Target-driven R&D in Japan (AS2511368P).
Correspondence to: Shuichi Matsuda (T: +81-75-751-3652; F: +81-75-751-8409; E-mail: smat522@kuhp.kyoto-u.ac.jp)

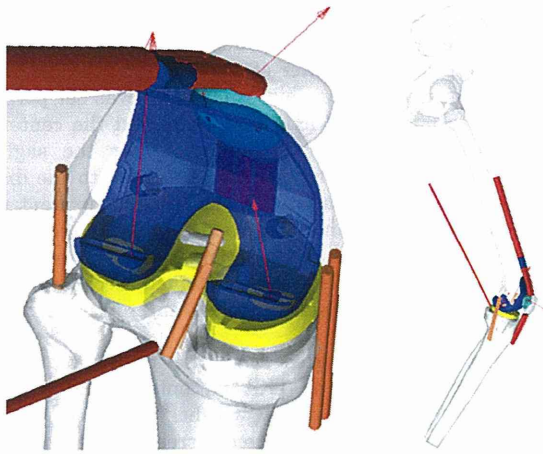

Figure 1. The ligament attachment points, the boundary conditions, and the model (including the hip and ankle joints) with neutral rotation of the standard tibial component.

between the tibial attachments of the anterior bundle and the posterior bundle, respectively (Fig. 1). The PCL comprised two bundles;[20,21] the femoral attachments were set on the anterior area of the medial intercondylar wall, and the tibial attachments were set on the posterior intercondylar fossa, anteroposteriorly in the order of anterior–lateral and posterior–medial bundles. The stiffness coefficients of LCL, MCL-anterior, MCL-posterior, and PCL were 59, 63, 63, and 204 N/mm, respectively, based on reported values.[14,21,22] The attachment and slack in each ligament in weight-bearing deep knee flexion were finely adjusted so that the length patterns were similar to those of a previous cadaver study (Fig. 2).[23]

The KneeSIM program uses Parasolid geometry for the femoral component, tibial insert, tibial tray, and patellar insert. Parasolid models of a fixed-bearing cruciate-retaining TKA (prototype for simulation; Kyocera, Kyoto, Japan) were imported into the model. The design of the femoral components has a single-radius sagittal geometry from 0°–90° (Fig. 3).

Three different constrained designs were constructed for the tibial inserts: (i) standard, (ii) high-constrained, and (iii) low-constrained. The basic geometry of each was the same; the main differences were the height of the anterior lip and the coronal geometry. The standard design had a low anterior lip, and the line connecting the deepest points of the articular surface in the coronal plane was straight in the AP direction (Fig. 4a). The rotational flexibility of the femoral component on this tray was limited to some extent by the intercondylar "eminence," and this design was similar to the geometry of the insert with the conventional design. The high-constrained design had almost identical coronal geometry to the standard insert but had a higher anterior lip (Fig. 4b). The low-constrained design had rotational flexibility; the line connecting the deepest points of the articular

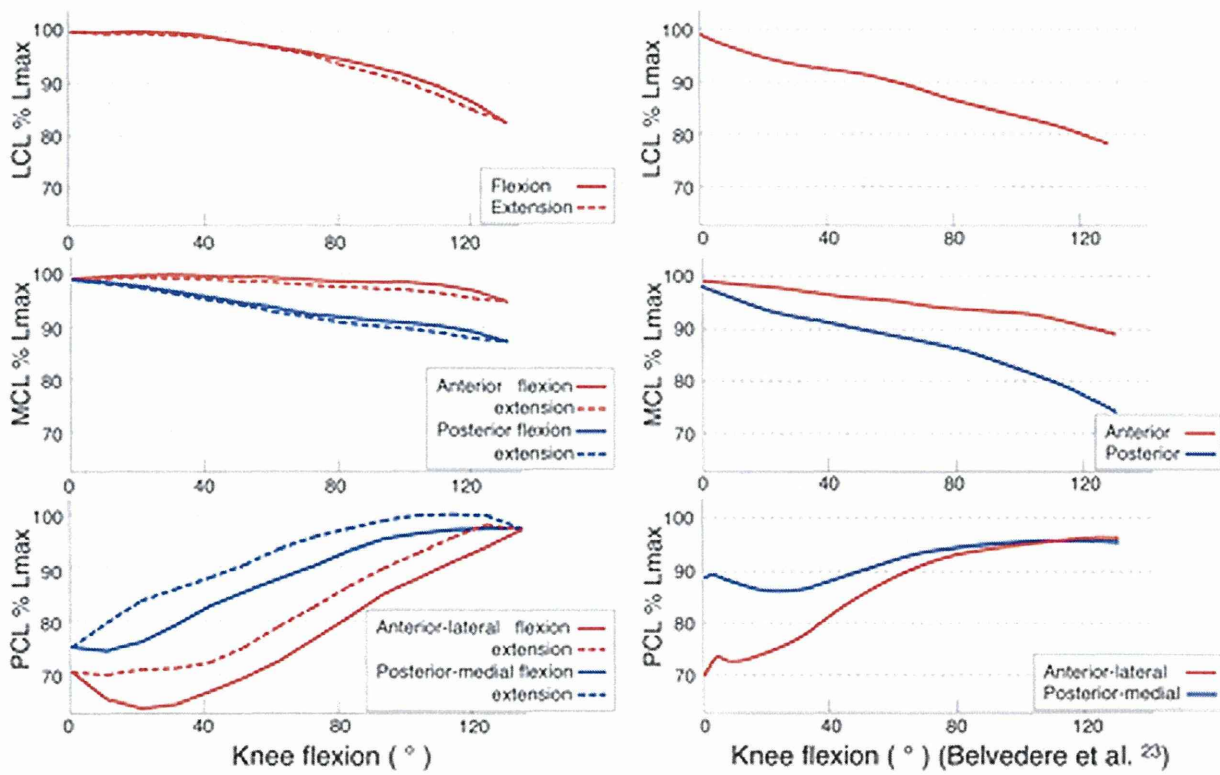

Figure 2. Left: The patterns of change in the translation length compared with each maximum length for the LCL, MCL, and PCL in weight-bearing deep knee flexion (0°–130°–0° flexion) (Lmax: the distance between corresponding attachments as a percentage of the corresponding maximum distance). Right: the LCL, MCL, and PCL length patterns reproduced from the cadaveric study of Belvedere et al.[23]